Report 2780

HYDRODYNAMIC LOADING AND CAVITATION ON FIXED AND ROTATING STRUTS OF 25 PERCENT THICKNESS

NAVAL SHIP RESEARCH AND DEVELOPMENT CENTER
Washington, D.C. 20007

HYDRODYNAMIC LOADING AND CAVITATION ON FIXED AND ROTATING STRUTS OF 25 PERCENT THICKNESS

by

David W. Coder

DEPARTMENT OF HYDROMECHANICS
RESEARCH AND DEVELOPMENT REPORT

December 1969

Report 2780

The Naval Ship Research and Development Center is a U.S. Navy center for laboratory effort directed at achieving improved sea and air vehicles. It was formed in March 1967 by merging the David Taylor Model Basin at Carderock, Maryland and the Marine Engineering Laboratory at Annapolis, Maryland. The Mine Defense Laboratory, Panama City, Florida became part of the Center in November 1967.

Naval Ship Research and Development Center
Washington, D.C. 20007

DEPARTMENT OF THE NAVY
NAVAL SHIP RESEARCH AND DEVELOPMENT CENTER
WASHINGTON, D. C. 20007

HYDRODYNAMIC LOADING AND CAVITATION ON FIXED AND ROTATING STRUTS OF 25 PERCENT THICKNESS

by

David W. Coder

December 1969 Report 2780

TABLE OF CONTENTS

LIST OF FIGURES

LIST OF TABLES

Page

NOTATION

A	Chordwise area of strut
C_D	Drag coefficient = $D/(1/2\ \rho\ V^2\ A)$
C_L	Lift coefficient = $L/(1/2\ \rho\ V^2\ A)$
C_N	Steady normal force coefficient = $N/(1/2\ \rho\ V^2\ A)$
$C_{N'}$	Unsteady normal force coefficient = $N'/(1/2\ \rho\ V^2\ A)$
C_T	Steady tangential force coefficient = $T/(1/2\ \rho\ V^2\ A)$
$C_{T'}$	Unsteady tangential force coefficient = $T'/(1/2\ \rho\ V^2\ A)$
c	Half-diameter of strut shaft
D	Drag
Fl	Forward-aft strain gage bridge
g	Gravitational acceleration
h	Depth of water
I	Area moment of inertia of strut shaft cross section about the diameter
L	Lift
M	Moment around base of strut due to steady normal force
N	Steady normal force
N'	Unsteady normal force
P_{atm}	Atmospheric pressure
P_v	Vapor pressure of water
P_1, P_2, P_3	Port-starboard strain gage bridges
P_∞	Absolute static pressure
s	Standard deviation
T	Steady tangential force
T'	Unsteady tangential force
V	Velocity of strut (or, equivalently, the free stream velocity)
X,Y	Dial indicator location coordinates shown in Figure 7
X',Y'	Profile offset coordinates shown in Figure 1
Y_p	Yield stress of strut material
1R	Rotating strut
1RM	Rotating strut modified

2F Fixed strut

3F Pinned rotating strut

3R Rotating strut

α Angle between model chord and the direction of the freestream velocity measured positive counterclockwise

ρ Density of the water

σ Cavitation number = $(P_\infty - P_v)/(1/2\ \rho\ V^2)$

ABSTRACT

Experimental results are presented for various towed struts of TMB-EPH cross section and thickness ratio of 25 percent. Force coefficients, strut accelerations, and cavitation characteristics as functions of velocity and angle of attack are given for a fixed strut of strong construction and a pinned rotating strut of weaker construction. The dynamics are given for rotating struts with axes of rotation at 18 percent chord with and without a splitter plate on the trailing edge. Test results obtained in fresh water at a depth of 1 ft are used to predict the behavior of the struts in sea water at a depth of 15 ft.

ADMINISTRATIVE INFORMATION

The work presented here was sponsored by the Bureau of Ships (now Naval Ship Systems Command - NAVSHIPS) under Project SS 048, Task 08543. The final report was prepared under NAVSHIPS Subproject S4606X, Task 1703.

INTRODUCTION

Several full-scale struts designed for installation on the USS PURVIS (DD 709) for the Conformal/Planar Array Sonar Program, were tested for seaworthiness and cavitation noise characteristics at the Naval Ship Research and Development Center. These struts, were supplied by TRG, Inc. and were instrumented and towed from Carriage 5 in the high-speed basin at speeds and angles of attack expected in full-scale conditions in the sea trials.

All of the struts were basically of a TMB-EPH shape; however, some were free to rotate and others were fixed. Cavitation conditions on the struts were determined by photographic methods. The maximum loads on the struts for the full-scale sea trials were predicted from the hydrodynamic tests. The struts were then statically loaded to determine whether they would fail under these maximum loading conditions.

This report describes the tests, presents the data, and discusses the feasibility of using the struts for shipboard installation.

TEST APPARATUS

All three of the struts tested had a basic TMB-EPH section as shown in Figure 1 with a basic chord length of 2 ft, a maximum thickness of

0.5 ft, a span length of 61 in., and a baseplate 20 in. in diameter and either 2 or 3 in. thick. The end of each strut was covered with a rounded endcap. Profile offsets are tabulated in Figure 1. The struts were numbered in sequence of their arrival and testing at NSRDC. The letter "F" or "R" after the strut number refers to a fixed or rotating test configuration. The struts differed mainly in their method of construction. Struts 1 and 3 were free to rotate in the flow around an axis located at 18 percent chord. These two struts rotated on bearings located at the top and bottom of a pivot pipe (4-in. outside diameter and 2.5-in. inside diameter) which extended from the baseplate. Strut 1 was tested freely rotating on its bearings. Strut 3 was tested both freely rotating and pinned to its baseplate with a 3/4-in.-diameter rod 8 1/2 in. aft of its axis of rotation. During testing, Strut 1R was found to have a divergent property. It was subsequently modified by attaching a 1- by 5-ft splitter plate on its trailing edge. This modification is denoted by the addition of the letter "M" to the strut code, thus making it Strut 1RM.

The basic difference between the two rotating struts is in the method of skin attachment. The skin of Strut 1 was welded on and that of Strut 3 was attached with screws. The torque required to overcome the friction in the bearings was measured by tying a string to the trailing edge of the strut and finding the torque required to turn it. This torque was found to be 30 ft lb for Strut 1R and 3 ft lb for Strut 3R. For the modified Strut 1RM, the clearance in the bearing was increased to change the required torque from 30 to 6 ft lb.

In addition to being fixed to its baseplate, Strut 2F differed in construction from the rotating struts. Whereas the skin of the rotating struts was 11-gage mild steel, the fixed strut was 3/8-in. 4130 steel (welded). The last 13 in. at the bottom of this strut was 14-gage stainless steel to provide an acoustic window for an enclosed hydrophone. A large EPH fairing was fitted on the top of Strut 2F in order to cover up triangular gussets (five on each side of the strut) located at the intersection of the strut and its baseplate. The physical characteristics of the struts are summarized in Table 1. The rotating struts were not designed to be as strong as the fixed strut because they were expected to

"follow" the flow and line up at all times at zero angle of attack. This would allow only drag forces which would be much smaller than the resultant of the lift and drag forces experienced by a fixed strut at an angle of attack.

An attachment known as the sonar destruction bridge and surface plate is available for use with Carriage 5 in the high speed basin. It was modified for these tests to permit the strut baseplates to be mounted flush with the bottom surface of the surface plate. The baseplates were mounted on a mechanism that allowed a ±18-deg change in angle of attack in increments of 3 deg from the top of the surface plate. When the bridge and plate were mounted on the carriage, the bottom of the surface plate was about 1 ft below the surface of the water.

A waterproof accelerometer package (Figure 2) was installed in the endcap of a strut during the test. This package enclosed three ±2g Statham accelerometers that were sensitive to acceleration in the vertical, port-starboard, and forward-aft directions, respectively.

The forces on the struts were determined by measuring the stress level at various locations on the struts during the hydrodynamic testing. Later, these stress levels were calibrated by applying static loads to the struts in air. To measure these stresses, Budd metalfilm strain gages, Type C6-141, were used in four active-arm bridges. Bridges sensitive to bending in the port-starboard direction were labeled with a "P" and those sensitive to bending in the forward-aft directions with an "F." Where more than one bridge was used in one of the directions, they were numbered starting from the baseplate toward the end of the strut. The locations of these bridges are shown in Figure 3. The sizes of the strain gages are exagerated for clarity. Half of the bridge (two gages) was mounted on either side of the bending surface. This surface was the skin of the fixed strut and the pivot pipe for the rotating struts. It was feasible to mount only port-starboard gages on the fixed strut. Bridge P2 was added onto the fixed strut for the structures test only. The rotating struts had a forward-aft bridge as well as port-starboard bridges.

Figure 4 shows a typical installation of a hydrophone (Atlantic Research Hydrophone LC-57) which was mounted in the bottom of each strut. Also shown is the angle of attack indicator used for the rotating struts.

One end of a piece of waxed chord was secured and wound around the hydrophone shaft. The other end was attached to the iron core of a linear variable differential transformer (LVDT). A negator kept a constant force of 1 lb on the other end of the iron core. Thus, as the strut rotated relative to the shaft which was fixed relative to the carriage, the iron core moved within the LVDT, causing a change in its mutual inductance. This change could then be calibrated as a function of angle of attack.

A Sanborn Model Series 350 Recorder was used to record the output of the strain gage bridges, the LVDT, and the accelerometers. The sound levels from the hydrophone were recorded on magnetic tape. During the testing, not all of these data were recorded for every strut. The information that was monitored during the test is listed in Table 1. High-speed, still, black and white photographs, both Polaroid and permanent, were made for each run through a window in the side of the basin.

TEST PROCEDURE

CARRIAGE TESTS

Tests were conducted in the high-speed basin on Carriage 5 in February 1966. Struts 1 and 1M were tested only as rotating struts. Strut 2 was fixed and Strut 3 was tested both fixed and rotating. Before each run, the angle of attack was set (for fixed struts only), water was allowed to settle at least 15 min, and the instrumentation was balanced. The water temperature was taken several times during the testing and was found to be 67 F $\pm$1. During each run, the velocity of the carriage was brought up to the desired velocity and held constant while the data were recorded. It was possible to obtain data for several velocities during many of the runs at low velocities. Above cavitation inception velocities, however, the velocity was held constant for the duration of the run since it was desirable to obtain a photograph at the viewing window for each velocity. In this way, only one cavitation condition would be tested per run. During successive runs, the velocity was increased in increments of about 5 knots up to the maximum permissible velocity depending on the strength of the strut and support mechanism. For the fixed struts, the angle of attack was varied from 0 to 18 deg in increments of 3 deg. One

additional set of runs for Strut 2F was made at a -6 deg angle of attack. The stress levels in the struts, as indicated by the strain gage bridges, were monitored during the test to ensure that the elastic limits of the struts were not exceeded.

Cavitation conditions were determined by examining the Polaroid photograph after each run. The carriage velocity was then varied to bracket the cavitation inception velocities.

Sound pressure levels from the hydrophone mounted in the bottom of the strut were also monitored during the test in the hope that some acoustical determination of cavitation inception could be made for comparison with the visual determination.

STRUCTURAL LOADING TEST

For calibration purposes, the hydrodynamic forces on the struts were assumed to be uniform along the span of the struts. The moment and stress near the base of the cantilever strut due to this uniform loading would be equivalent to the moment and stress due to the total load located at midspan. Thus, the struts were calibrated (with the assistance of the Structural Mechanics Laboratory) by statically loading them in a cantilever manner at midchord. The 600,000-lb testing machine was used to apply the force. A soft wood loading block covering 1-ft span of the side of the strut was centered around midspan as shown in Figure 5. It had been felt that uniform loading would be better approximated by using two additional loading blocks identical to the first and placed one on each side of the first. However, the loading block of the machine was not free to pivot as the strut bent under the load. This caused the total force to be applied further and further toward the mounted end as the load increased, resulting in a reduction in moment and stress due to the same total force from the "one block" system to the "three block" system. For this reason, it is felt that the data using one loading block better represented the stresses obtained from hydrodynamic loading.

Dial gages measuring to 0.001 in. were placed at various locations on the struts and base as shown in Figures 5 and 6. Figure 7 gives the exact locations of the dial gages for the various struts. Strut 3F was loaded to a maximum of 9000 lb in 1000-lb increments using one loading

block placed at its midspan as shown in Figure 5. Two additional loading blocks, identical to the first, were placed one on each side of the initial one and the strut was retested to a maximum of 8000 lb. Strut 2F was loaded to a maximum of 60,000 lb (in 5000-lb increments, returning to zero between each load increase) using one loading block. The thinner end section of the strut was tested with one loading block to a maximum of 12,000 lb (in 1000-lb increments, returning to zero between each load increase). Data taken for equivalent configurations were repeatable within less than 5 percent. Thus, for clarity, only representative data are presented in Figures 8 through 11 and Tables 2 through 5.

The strain levels on the pinned rotating strut (Strut 3F) were measured by strain gage Bridges P1, P2, P3, and F1 on the pivot pipe which supported the strut. There was a very nearly linear increase in strain in the port-starboard Bridges P1, P2, and P3 with load during loading; see Figures 8 and 9. During unloading, a hysteresis effect was noticed. The strain lagged behind the load but then approached zero as the load approached zero.

The calibration apparatus allowed loads to be applied to the strut to create bending in the port-starboard direction only. The forward-aft strains shown in Figures 8c and 9c for Bridge F1 represent interactions in the calibration technique since no force was applied in this direction. It is seen that the interaction strain in the forward-aft Bridge F1 was typically less than 10 percent of the port-starboard Bridge P1 at the same location.

No provision was made to load the struts in the forward-aft direction in order to calibrate Bridge F1. However, it was assumed that calibrations made for P1 could be used for F1, which was located at approximately the same distance from the endplate but 90 deg from P1.

The strain levels on fixed Strut 2F were measured by strain gage Bridges P1 and P2 on the skin of the strut. The results indicate a linear increase in stress with load as shown in Figures 10 and 11. No hysteresis effects were observable because of the method of testing.

The calibration curves that were used to determine the hydrodynamic loads are shown as dashed lines on Figures 8a and 10. Bridge P2 was used for Strut 3F since P1 failed to operate properly during the hydrodynamic test.

The actual loading deflections of the strut, which were obtained by the dial indicators, are given in Tables 2 through 5. Because the base which held the struts deformed slightly with load, these values of deflections could be corrected for deflections relative to the base. These corrections could be obtained by assuming that the base shift resulted in a twist about the horizontal axis "Y" on the plane of symmetry of the strut as shown in Figure 7. Therefore, the corrections were made by assuming rigid body motion around this axis and using the deflections of Indicator 8. Corrected values for Strut 3F are also included in the tables.

RESULTS

ROTATING STRUTS

Strut 1R demonstrated that the rotating struts would not follow the flow as expected but assumed some angle to the flow as determined by the velocity. At this angle, the hydrodynamic moment acting on the foil balanced the friction in the bearings. It was difficult to determine this angle-velocity relationship for Strut 1R. A large velocity was required to produce a large enough hydrodynamic moment to overcome the bearing friction torque and turn the strut. Also it would not turn continuously with increasing velocity but would suddenly jump to the new angle of attack. As the velocity is increased beyond 15 knots, cavitation will occur on the body of the strut at some velocity and resulting angle of attack. When strut cavitation occurs, the angle of attack is suddenly reduced because of a change in loading and the cavity is washed off. Then the angle increases again and the cycle is repeated. For a velocity of about 20 knots and test depth, it was found that Strut 1R oscillated between 26- and 15-deg angle of attack at a frequency of about 5.5 cps with cavitation alternately appearing and disappearing. It was feared that this uncontrollable, sudden increase in angle of attack and vibration would cause excessively high loads on the strut and mounting mechanism. Thus it was decided to modify Strut 1 by loosening the bearing and by fitting a splitter plate on its trailing edge in an attempt to stabilize it.

The test results for the rotating strut modified with a splitter plate (Strut 1RM) indicate that starting from any angle of attack, the foil

assumes an angle of attack of approximately zero. This is true for any velocity up to about 33 knots. At this velocity and at test depth, cavitation on the body begins and violent oscillations result.

Since Strut 3R required a smaller moment to change the angle of attack, the hope was that it would assume a zero angle of attack when preset at any angle. This would reduce cavitation and hold hydrodynamic loading to a minimum. The test showed, however, that this strut stabilized at ever-increasing angles of attack; see Figure 12. This divergent effect may be due to the center of pressure being forward of the 18 percent chord line to the three-dimensional effect of drag moment resulting from bending of the foil. For a detailed discussion of divergence see, for example, Reference 1.* As a result of the increase in angle of attack which was found, the loading on the strut and its vibrations were much larger than were considered in the original strut design. For example, if one assumes a normal force coefficient of 1.0 for large angles of attack and a velocity of 30 knots, the stress on the strut would be 156×10^3 psi or more than twice the yield stress for the high-strength shaft.

During the hydrodynamic test of Strut 3R, it was observed that the skin of the strut had several cracks and pin holes. No additional hydrodynamic tests were made with that strut for fear of destroying it. It was felt that the cracks were due either to poor welding or to the intense overload and cavitation conditions which caused severe vibrations during testing.

Accelerometer data for the rotating struts are given in Figure 13. Note that the accelerations of Strut 1RM were considerably lower than either Strut 1R or 3R in the port-starboard and forward-aft directions. Thus the splitter plate not only stabilized the strut but also reduced its vibration.

*References are listed on page 59.

FIXED STRUTS

The two fixed struts, 2F and 3F, had identical geometries except for the fairing at the root of Strut 2. This fairing obviously changed the cavitation characteristics of the flow near the root and may have been responsible for some of the differences observed in the measured force coefficients and cavitation conditions along the struts. Another difference in force coefficients could be due to the calibration technique. No force measurements were made on the 3/4-in.-diameter pin between the strut and baseplate which carried part of the load of Strut 3F. If the calibration loads were not placed exactly at the hydrodynamic center of the pressure, the pin would carry a different percentage of the load during calibration than during the hydrodynamic test. The amount of error due to this technique is not known. Thus it would seem that the data for Strut 2F would be more reliable as far as forces are concerned.

Strut 3F was constructed lighter than Strut 2F and unfortunately could not be tested under a wide variety of conditions for fear of overstressing the strut shaft.

Steady Forces

The calibration curves obtained from the structural test were used to determine from the Sanborn records the steady forces normal and tangential to the strut. These values were nondimensionalized as force coefficients by dividing them by the dynamic head times the chordwise area. For a given angle of attack, the steady force coefficients had no apparent variation with velocity. Thus average values over the entire velocity range and their associated standard deviations were computed for each angle of attack and plotted as shown in Figures 14 and 15. These figures indicate an almost linear increase in steady normal force coefficient with angle of attack for both fixed struts. It is also seen that the true hydrodynamic zero angle of attack occurred at about +0.4 deg for Strut 2F and -0.6 deg for 3F. If these two figures are superimposed at this true zero angle of attack, it is seen that the steady normal force coefficient was smaller for Strut 3F than for Strut 2F.

Tangential forces were measured only on Strut 3F since these measurements could be made easily on this strut. Figure 15b shows the steady tangential force coefficient as determined with Strut 3F. It is seen that the steady tangential force became negative, or was directed toward the leading edge of the strut, for angles greater than about 3.4 deg.

Drag and lift coefficients could be obtained from these data using the equations

$$C_D = C_T \cos \alpha + C_N \sin \alpha$$

$$C_L = C_N \cos \alpha - C_T \sin \alpha$$

where

C_D is the drag coefficient,
C_L is the lift coefficient,
C_T is the steady tangential force coefficient,
C_N is the steady normal force coefficient, and
α is the angle of attack.

From the tests on the fixed struts, the largest steady normal force coefficient was found to be 1.1 at 18 deg. Using a velocity of 35 knots, this results in a total steady normal force of about 38,500 lb. This load produced a stress level of 19.25×10^3 psi at the root of Strut 2F where the gussets were located. Since the yield stress of the strut material was assumed to be 60×10^3 psi, there was ample safety factor to take account of dynamic loading and cavitation loading which would be something less than twice the static load.

Because unsteady forces are greatly influenced by cavitation, their discussion will be postponed until after the introduction of that subject.

Cavitation Characteristics

The types of cavitation on Struts 2F and 3F are shown in Figures 16 and 17, respectively, and a summary of cavitation inception velocities at the test depth versus angle of attack is given in Figure 18. For small angles of attack, the first cavitation to occur as the velocity is

increased is what has been labeled "root" cavitation. This appears on Strut 2F as a cloud of bubbles extending aft from about the three-quarter chord near the root of the strut; see Figure 16a. It is felt that this is a mixture of cavitation on the strut and air coming out of solution as a result of the cavitation and remaining after the collapse of the cavitation bubble. This phenomenon has been observed before in a rudder test; see Figures 10 through 14 of Reference 2. "Root" cavitation on Strut 3F is shown in Figure 17a. A comparison of "root" cavitation summaries for the two fixed struts on Figure 18 indicates that this cavitation typically occurred approximately 5 knots higher for Strut 3F except near zero angle of attack. This indicates that the fairing on Strut 2F evidently delayed "root" cavitation for small angles of attack (less than about 2 deg) but promoted it for larger angles.

An additional type of cavitation was observed on the fairing of Strut 2F. When the cavitation on the fairing jumps forward from the three-quarter to the one-quarter chord point, this is referred to as "root forward" cavitation and is shown in Figure 16b. It must be noted that at both the three-quarter and the one-quarter chord points, slight discontinuities were detected in the surface of the fairing and these no doubt triggered cavitation.

Spanwise cavitation is referred to as "strut" cavitation and is shown on Figures 16b and 16c for Strut 2F and on Figures 17b and 17c for Strut 3F. "Strut" cavitation at zero angle of attack occurred just aft of the maximum section of the struts as shown in Figures 16b and 17b. It first appeared at a velocity of 37 knots for Strut 3F and 34 knots for Strut 2F. Unfortunately "strut" cavitation could not be obtained for other angles for Strut 3F because of the high hydrodynamic loads that would be generated. For angles of 3 deg or greater, "strut" cavitation starts from near the leading edge as shown in Figure 16c.

Cavitation in the tip vortex aft of the rounded end section is referred to as "tip vortex" cavitation and is shown in Figure 16c for Strut 2F and in Figure 17a for Strut 3F. This type of cavitation could be obtained under safe conditions for both struts. The results summarized in Figure 18 show that this cavitation occurred at approximately the same velocity for both struts except near 9 deg where Strut 3F cavitated at a velocity about 5 knots lower.

As shown in Figure 18, the general trend for all types of cavitation is that the cavitation inception velocities are reduced as the angle of attack is increased. The first type of cavitation to be observed as the velocity increases is "root" cavitation or "tip vortex" depending on whether or not the strut has a fairing and also on the angle of attack. The fairing on Strut 2F reduced the "root" cavitation inception velocity sufficiently so that this type of cavitation occurred first for all of the angles tested. On Strut 3F, however, "tip vortex" cavitation occurred before "root" cavitation for angles of 12 deg and greater.

On Strut 2F, "root forward" cavitation occurred before "strut" cavitation for angles less than 6 deg. For angles greater than 6 deg, the order was reversed. The "tip vortex" cavitation first appeared at 9 deg and come in ahead of "root forward" and "strut" cavitation at all angles greater than 11 deg.

So far as cavitation is concerned, adding the splitter plate to the profile reduced the "root" cavitation inception velocity to about 6 knots! Possibly this was caused by the longer sharp edge on the top of the strut. The "strut" cavitation inception velocity remained about the same at 33.5 knots for Strut 1RM.

As stated before, an attempt was made to obtain acoustically an absolute measure of the inception of cavitation of the struts. Acoustical data were obtained by recording the output of the hydrophone during each run. Unfortunately, the rigid mounting of the hydrophone within the strut precluded any measurement of sound pressure levels because of excessive strut vibrations. It is felt that if these struts are to be employed as housings for hydrophones, a mounting device should be used to reduce the vibrations transmitted to the hydrophone.

Unsteady Forces

The force traces on the Sanborn recorders can be considered as composed of two parts. The steady part, or average displacement from zero, has been referred to as the steady force. Oscillating around this average displacement was another signal which could be referred to as an unsteady force. The amplitude, or peak-to-peak value, of this superimposed oscillating signal often varied randomly or in a beating manner. One-half

of the maximum peak-to-peak signal that was seen to repeat several times is hereafter referred to as the half-amplitude of the unsteady force. This force was nondimensionalized, as was the steady force, by dividing it by the dynamic head times the chordwise area.

The unsteady force coefficients (Figures 19, 20, and 21) seem to be very much a function of both velocity and angle of attack. The unsteady forces at low velocities are due to the alternating pressure fields as vortices are shed from the trailing edge of the strut. It is noticeable that for all angles of attack, there is a general decrease in unsteady force coefficients as the velocity is increased. This indicates that the energy going into vortex formation is becoming a smaller percentage of the total available energy, i.e., the free-stream kinetic energy. The curves then tend to flatten out at about an unsteady normal force coefficient of about 0.01 and an unsteady tangential force coefficient of about 0.002.

The point of departure from this leveling out point depends on angle of attack. It turns out that this point of departure is the "strut" cavitation inception velocity for that particular angle. At this point, the unsteady normal force coefficient increases sharply as the velocity is further increased. Thus, cavitation on the body of the strut results in a sudden increase in the dynamic loading on the strut. Although Strut 3F was not tested at angles other than zero, it is expected that the points of departure for angles other than zero would be the "strut" cavitation inception velocity for that particular angle. This general tendency is indicated on Figures 20 and 21 by dashed lines.

Strut Accelerations

Further information on the dynamics of the struts is obtainable from the accelerometers mounted in the endcap. Half peak-to-peak values of the maximum accelerations were read from the Sanborn traces. The accelerometer package was not included in the endcap of Strut 2F during testing above 15 knots. Data below 15 knots showed considerable scatter and were very similar both in amplitude and frequency to data shown in Figure 22 for Strut 3F.

It is reasonable to assume that these accelerations would be proportional to their forcing function--namely the unsteady hydrodynamic forces. Thus, if the accelerations are nondimensionalized by multiplying them by a unit mass and dividing them by the dynamic head times the area, then when this acceleration coefficient is plotted versus velocity, the resulting graph should be similar to those for the unsteady force coefficients. This has been done for the Strut 3F data as shown in Figure 23. A comparison of Figure 23b with Figure 20 and Figure 23c with Figure 21 indicates that the graphs are similar for zero angle of attack. This means that when cavitation occurs on the strut, the unsteady force coefficients and resulting strut acceleration coefficients suddenly increase. Here again the assumption could be made that the sudden increase in acceleration coefficient occurs near the "strut" cavitation inception velocity for the various angles of attack. This is shown as dotted lines on Figure 23.

PREDICTION OF STRUT BEHAVIOR IN FULL SCALE TRIALS

The TRG struts were prototypes of the struts to be used for a shipboard experiment. The proposed operating depth of the struts is about 15 ft. The flow field around the bottom of the ship in which these struts are to be used is not well defined. It would be necessary to study this flow field in order to accurately predict behavior when the struts are installed on the ship. However, it is not the purpose of this report to study the ship-strut system. It will be assumed that the strut on the ship is exposed to uniform flow along its span except for a small boundary layer near the root of the strut. Also, the alignment on the ship would be such as to have the strut at 0 deg to the flow when the ship is proceeding forward without rolling. Turning of the ship and rolling velocities combined with forward velocities would change the flow field relative to the strut. An attempt has been made to allow for these conditions by testing the fixed struts up to an angle of attack of 18 deg. Since the struts were full sized and the flow field has been assumed the same, the differences from the model tests to full-scale installation on the ship would be a result of operation in sea water instead of fresh water and operation at a different depth.

The density of sea water is about 3 percent greater than that of fresh water. Thus, if one assumes that the force coefficients would remain the same as for the model tests, operation in sea water would give forces that are approximately 3 percent greater. The effect of sea water on cavitation conditions results from changes in vapor pressure as well as density changes. The vapor pressure of sea water is approximately 2 percent less than that of pure water at the same temperature (page 67 of Reference 3). The nondimensional number used to predict cavitation behavior is the cavitation number and is defined as

$$\sigma = \frac{P_\infty - P_v}{1/2\ \rho\ V^2}$$

where P_∞ is the absolute static pressure,
P_v is the vapor pressure of the water,
ρ is the density of the water, and
V is the free-stream velocity.

If the cavitation number is differentiated and divided by itself, it is found that

$$\frac{d\sigma}{\sigma} = \frac{d(P_\infty - P_v)}{P_\infty - P_v} - 2\frac{dV}{V} - \frac{d\rho}{\rho}$$

In other words, the percentage change in σ from the model test to the full-scale test is equal to the percentage change of $(P_\infty - P_v)$ less twice the percentage change in velocity less the percentage change of density. Earlier it was assumed that the velocity would not change; thus

$$\frac{d\sigma}{\sigma} = \frac{d(P_\infty - P_v)}{P_\infty - P_v} - \frac{d\rho}{\rho}$$

The absolute static pressure may be separated into two parts so that

$$P_\infty = P_{atm} + \rho gh$$

where P_{atm} is the atmospheric pressure,
g is the gravitational acceleration, and
h is the depth of water.

Then, assuming that the atmospheric pressure remains constant and holding the depth fixed, we see that

$$\frac{dP_\infty}{P_\infty} = \frac{d\rho}{\rho}$$

Substituting this relation into the above expression for $d\sigma/\sigma$, we obtain

$$\frac{d\sigma}{\sigma} = \frac{d\rho}{\rho}\left(\frac{P_v}{P_\infty - P_v}\right) - \frac{dP_v}{P_v}\left(\frac{P_v}{P_\infty - P_v}\right)$$

Now if we assume $d\rho/\rho = 0.03$ and $dP_v/P_v = -0.02$, we see that

$$\frac{d\sigma}{\sigma} = 0.05\left(\frac{P_v}{P_\infty - P_v}\right)$$

Atmospheric pressure is about 14.7 psi at sea level and the vapor pressure for water up to 80 F is less than 0.5 psi so that

$$\frac{d\sigma}{\sigma} < 0.0022$$

for temperatures less than 80 F. It is seen from the preceding analysis that the changes in vapor pressure and density due to salinity do not change the cavitation number significantly.

It will now be seen that depth represents the major difference between the shipboard installation and the model test. Since the struts were tested at a depth of only 1 ft, it is necessary to determine the effects of additional depth on the test results. For the fully wetted (i.e., noncavitating) strut, it is expected that the pressure coefficient at any point in the flow field would not change with depth. The steady force coefficients, unsteady force coefficients, and strut acceleration would not change with depth for the fully wetted strut since they are functions only of the pressure coefficient.

The change in depth does, however, change the absolute pressure in the flow field. One would find then, that the deeper the depth, the higher the pressure and the less the likelihood of cavitation. Thus, cavitation

inception velocities would increase as the depth is increased. The data summarized in Figure 18 for the test depth of 1 ft, using the top of strut as a reference, may be converted to results for any depth by use of the cavitation nomograph shown in Figure 24. The inception velocity and the test depth will give a corresponding cavitation index (critical cavitation number). It is assumed that this index would remain constant for a given shape and angle. This then can be used to obtain an inception velocity at any depth. This has been done in Figure 25 for the depth expected on PURVIS, namely 15 ft.

It is seen from the above discussion that the sudden increase in the unsteady force coefficients and acceleration coefficients due to cavitation would be delayed to a higher velocity for the greater depth. For example, the unsteady force coefficients and accelerations for the struts at zero angle of attack would not start increasing until about 40 knots for a depth of 15 ft instead of about 34 knots for 1 ft.

CONCLUSIONS AND RECOMMENDATIONS

It was found that struts of TMB-EPH profile that are free to pivot about 18 percent chord will not line up at zero angle of attack to the flow but will assume some angle to the flow. This angle increases with increasing velocity. This divergent property defeats the purpose of the design, which is to minimize hydrodynamic loading and cavitation. The strut may be stabilized by ensuring that the center of pressure is aft of the axis of rotation. This will cause the strut to rotate until it lines up at 0 deg to the flow. The addition of a splitter plate on the trailing edge of the strut also causes this shift in the center of pressure to stabilize the strut.

Unfortunately, the addition of the splitter plate makes the cavitation conditions near the root of the strut more severe. Thus the rotating strut with a splitter plate would have little use in a system in which cavitation noise is to be kept to a minimum. For systems in which cavitation noise is not a problem, a stable rotating strut would have at least two advantages over a fixed strut: (1) it could be constructed lighter than a fixed strut because of the absence of a lift force and (2) the initial alignment on the ship would not be a problem since the strut seeks its own alignment.

If the cavitation problem at the top of the strut could be solved, a stable rotating strut is considered superior to a fixed strut because of the factors listed above plus at least one additional advantage. The stable rotating strut with improved cavitation conditions could be used for full-time operation on a ship that is turning and/or rolling without much change in self-induced noise. On the other hand, the relative flow field would change for the fixed strut and thus the resulting self-noise would change. In this case, perhaps only part instead of the whole roll cycle could be used for efficient acoustic operation with the fixed strut. An attempt could be made to reduce cavitation at the top of rotating struts by rounding the sharp edges at the top. It is possible that the whole top of the strut could have a radius similar to that of the endcap at the other end. It must be remembered that doing this would change the flow field near the top of the strut, and the resulting intersection vortex could possibly make cavitation conditions even more severe.

It was found that the normal force coefficient for the fixed strut varies almost linearly with angle of attack up to a value of about 1.1 at 18 deg. Using this value, it is seen that the strut could easily stand any hydrodynamic loading up to 35 knots. Near zero angle of attack, no types of cavitation occur up to about 35 knots. Also, it is felt that cavitation on the fairing might be reduced by redesigning the fairing so that its maximum thickness would be located at the same chordside distance as that of the strut itself. This would match the minimum pressure point on the fairing with that of the strut and might reduce the intersection vortex. Also, fairing directly onto the ship and finishing the fairing to reduce sharp edges and rough surfaces would help reduce the onset of cavitation.

Until the problem relating to the cavitation on the top of the rotating struts is worked out, it is recommended that the fixed strut be used for operations where cavitation noise is undesirable.

ACKNOWLEDGMENTS

The author gratefully acknowledges the assistance of several staff members, particularly Mr. D.A. Shaffer who greatly assisted in designing and conducting the test. Messrs. L.B. Moore and E.P. Rood helped to conduct the tests and the latter also reduced all the raw data. The structures test was conducted by Mr. P. Yarnall under the supervision of Mr. L. Becker of the Department of Structural Mechanics. That department also provided personnel to design the test rig, to run the testing machine, and to help conduct the test. However personnel of the Fluid Dynamics Branch, Department of Hydromechanics, specified the loads and recorded the resulting data. Mr. J.C. Olive of the Department of Acoustics and Vibration handled the acoustics part of the test and Messrs. T.P. Tehan and C. Eckloff of the Instrumentation Division, Office of the Technical Director, handled the instrumentation of the struts.

Finally, thanks are due Mr. N. Weingart of TRG, Inc. for the several valuable suggestions he made before and during the test.

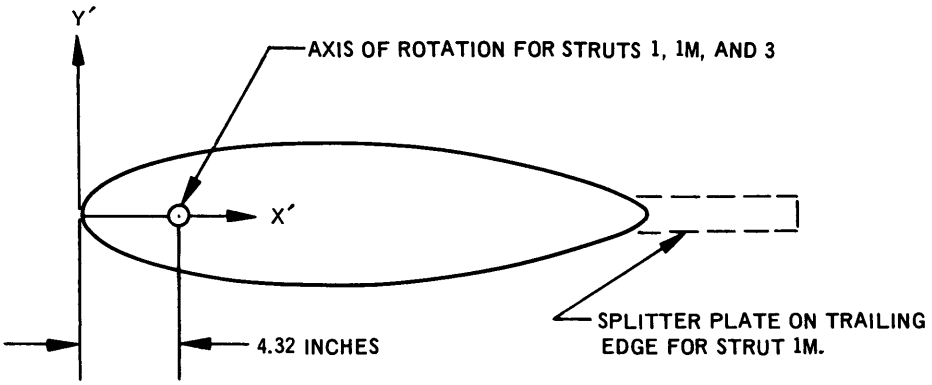

SHAPE = TMB–EPH
SPAN = 61 INCHES
CHORD = { 2 FT FOR STRUTS 1, 2, AND 3
= { 3 FT FOR STRUT 1M
THICKNESS = 1/2 FT

X′ inches	Y′ inches	X′ inches	Y′ inches
0.00	0.00	12.00	2.97
0.12	0.45	13.20	2.90
0.24	0.64	14.40	2.79
0.48	0.90	15.60	2.64
0.96	1.26	16.80	2.45
1.68	1.63	18.00	2.22
2.40	1.91	19.20	1.96
3.60	2.26	20.40	1.65
4.80	2.52	21.60	1.30
6.00	2.71	22.32	1.07
7.20	2.85	22.80	0.89
8.40	2.94	23.28	0.68
9.60	2.99	23.76	0.39
10.80	3.00	24.00	0.00

Figure 1 - Profiles of Struts with Coordinates of Outside Dimensions of Basic Shape

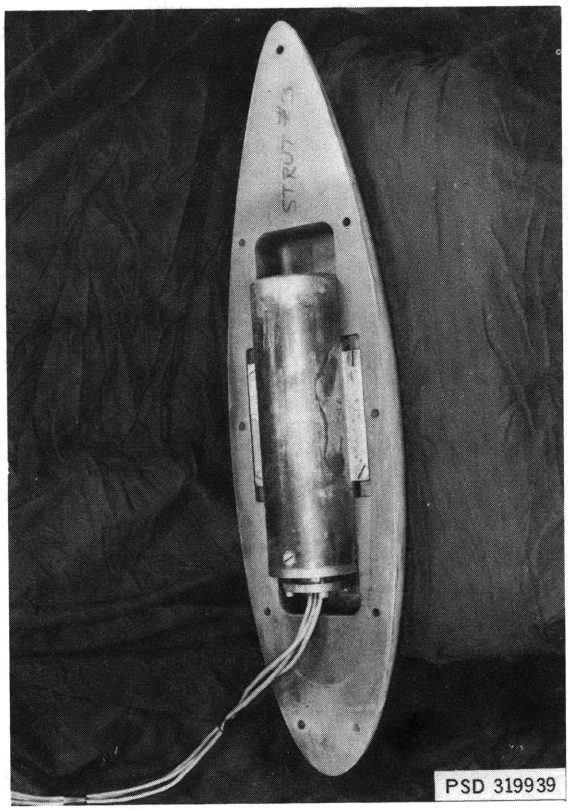

Figure 2 - Strut Endcap Showing Accelerometer Package

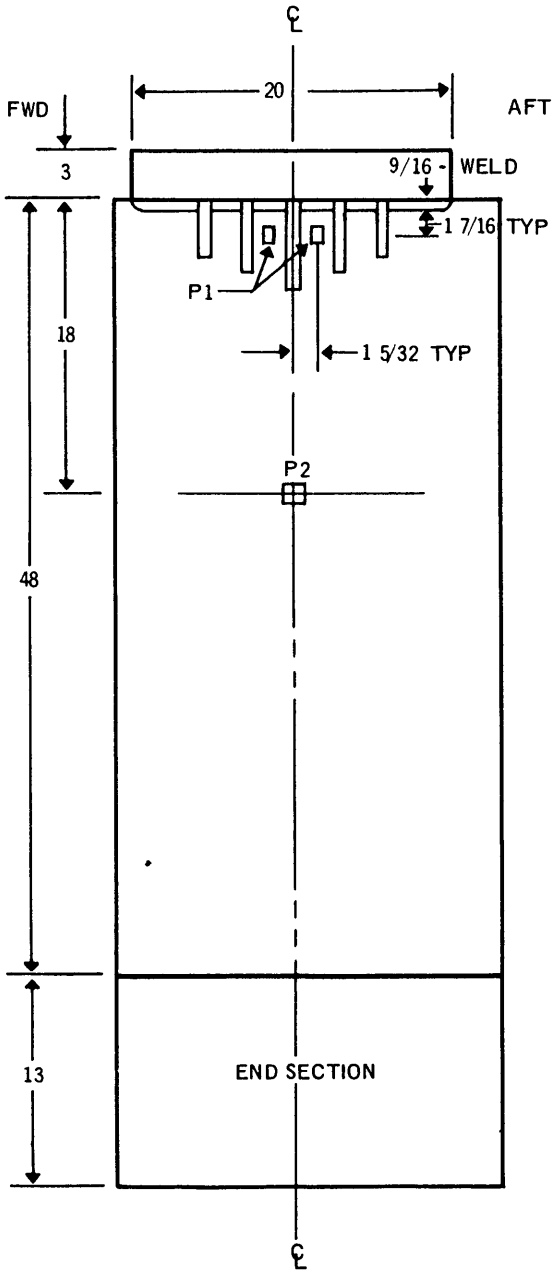

Figure 3a – Location on Skin of Fixed Strut

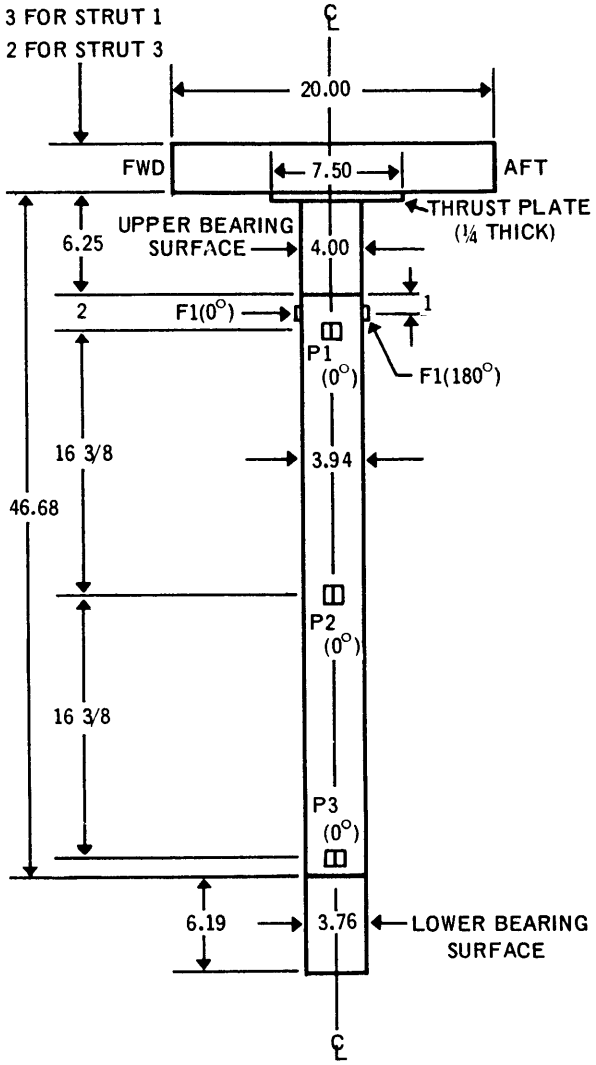

Figure 3b – Location on Pivot Pipe of Rotating Struts

Figure 3 - Strain Gage Bridge Locations

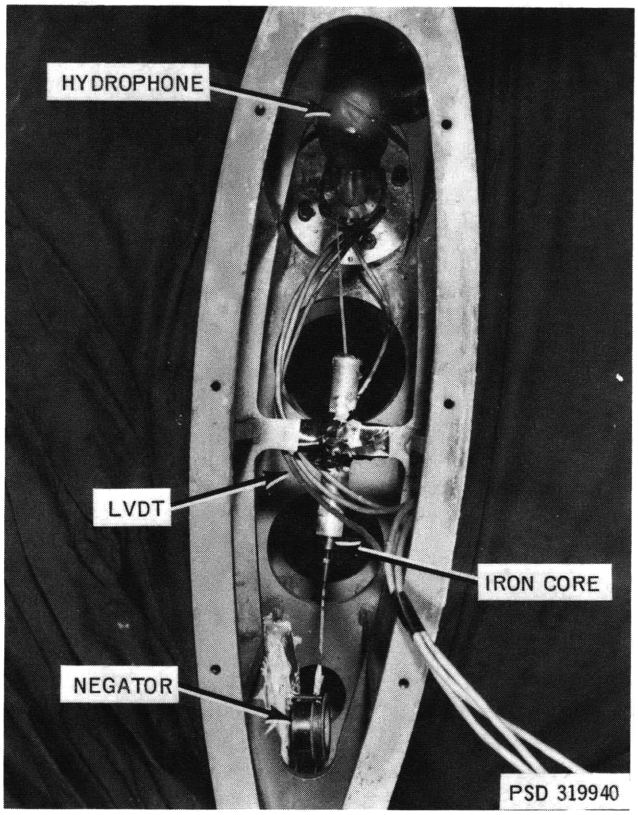

Figure 4 - Bottom View of a Rotating Strut with Endcap Removed to Show Hydrophone Location and Angle of Attack Indicator

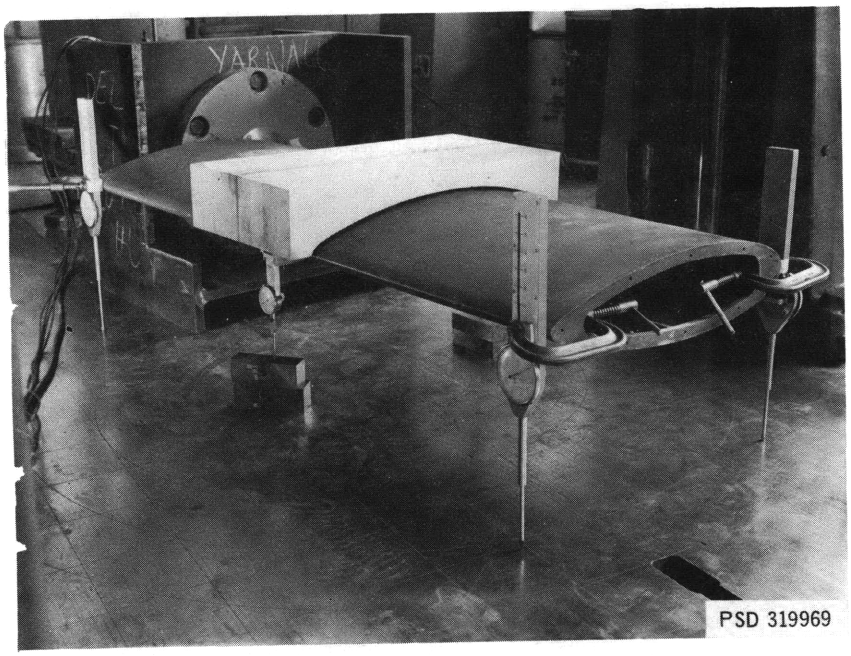

Figure 5 - Strut 3F Ready for Structural Loading Test with One Loading Block

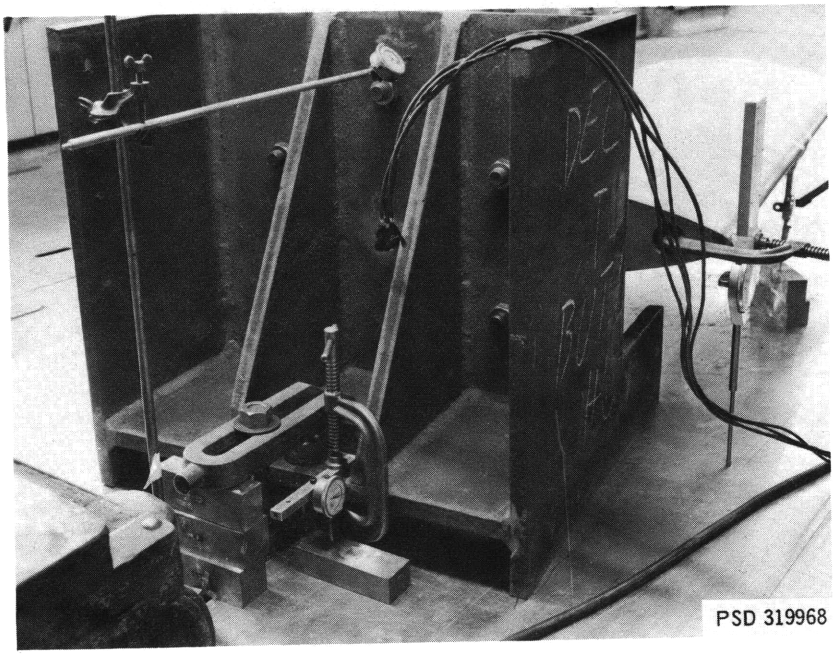

Figure 6 - Base Used to Mount Struts for Structural Loading Test

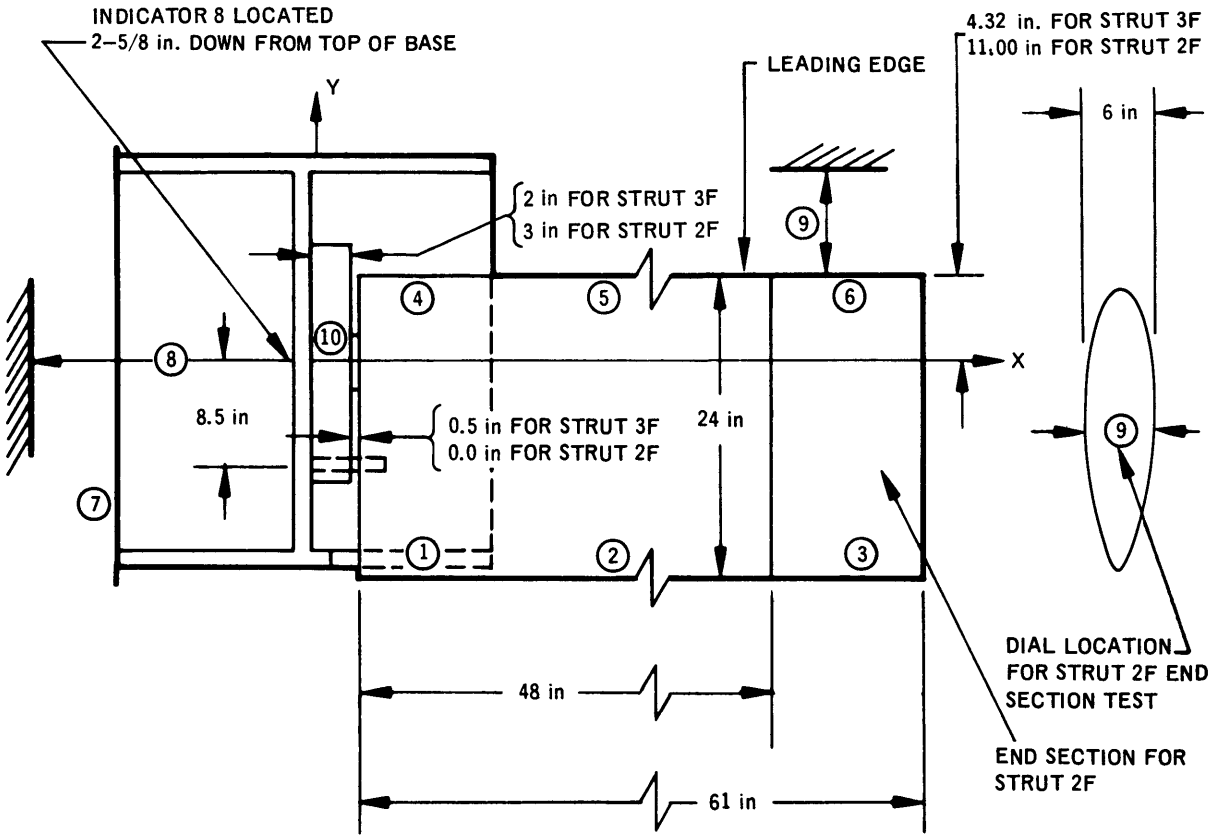

Indicator Number	STRUT 3F TEST		STRUT 2F TEST		STRUT 2F END SECTION TEST	
	X inches	Y inches	X inches	Y inches	X inches	Y inches
1	3.19	-20.24	17.00	-13.56	33.00	-13.50
2	33.00	-18.68	33.50	-12.50	52.50	-12.50
3	61.94	-20.24	64.38	-13.00	64.50	-11.00
4	3.94	3.13	17.00	10.50	29.50	11.50
5	33.00	3.13	33.50	10.50	52.50	10.50
6	63.25	4.82	64.38	9.12	64.50	9.00
7	− 13.50	- 7.47	− 13.50	- 7.47	− 13.50	- 7.47
8	− 1.00	0.00	− 1.00	0.00	− 1.00	0.00
9	62.00	4.32	61.00	11.00	64.00	0. 00
10			0.00	0.00	0.00	0.00

Figure 7 - Dial Indicator Locations for Structural Loading Test

Figure 8 - Strain on Pivot Pipe versus Load for Strut 3F with One Loading Block

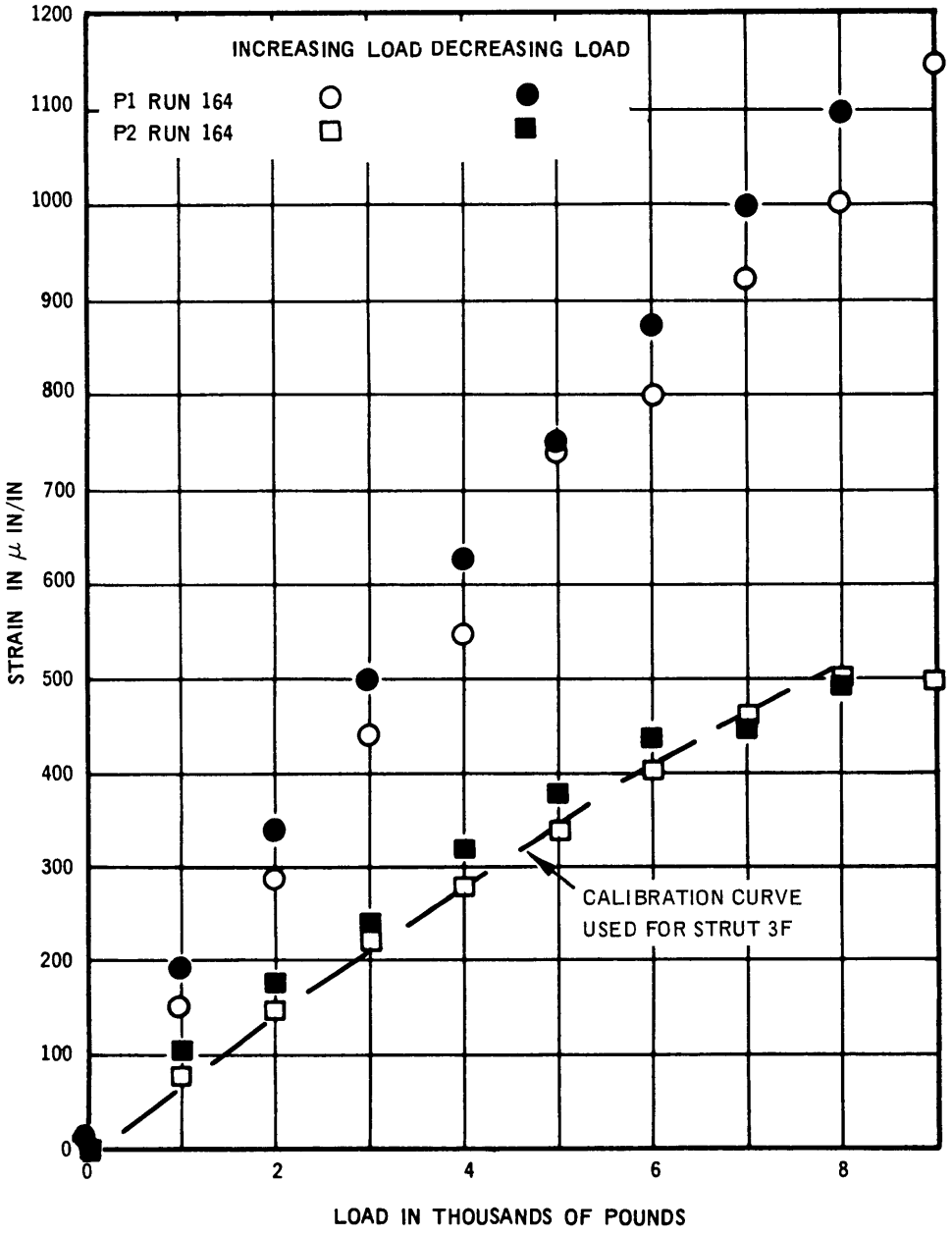

Figure 8a – Gages P1 and P2

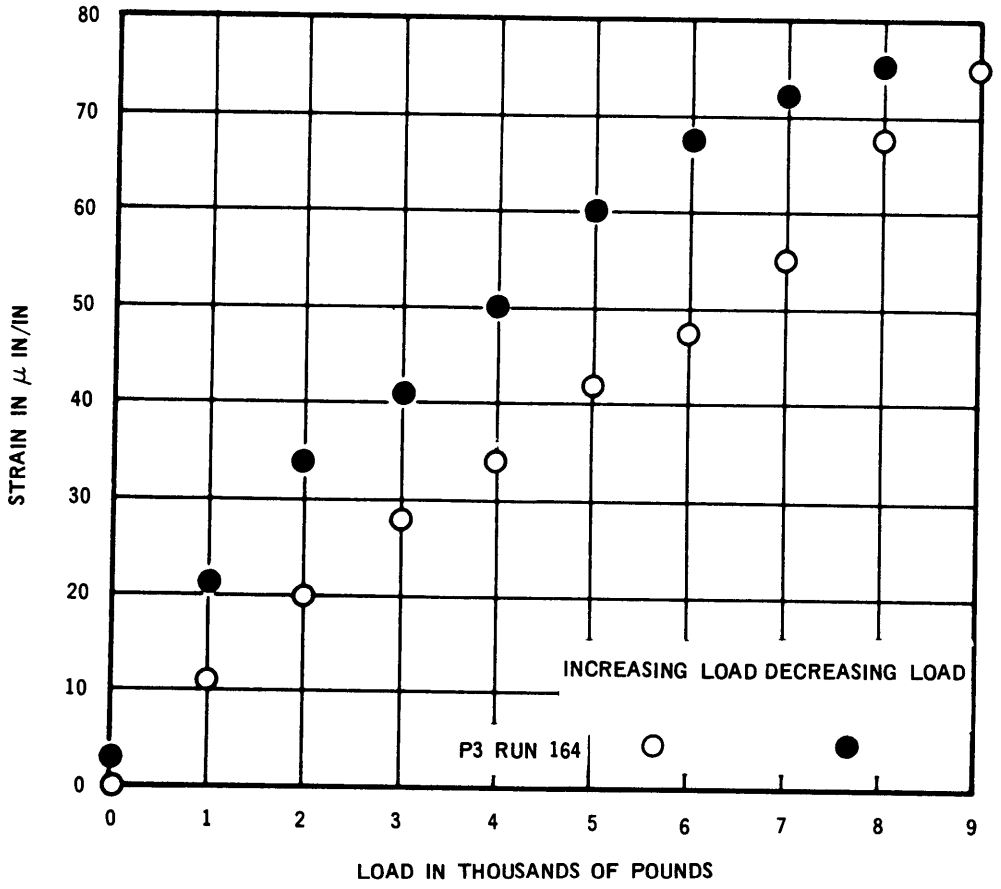

Figure 8b – Gage P3

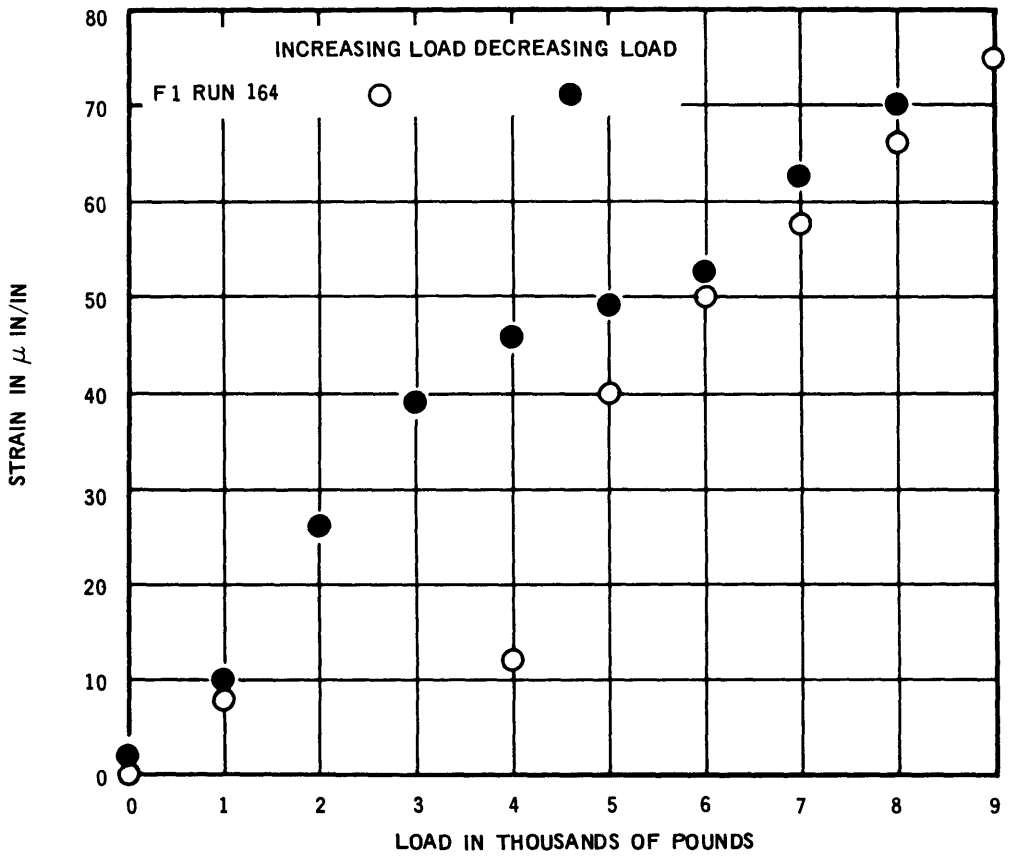

Figure 8c – Gage F1

Figure 9 - Strain on Pivot Pipe versus Load for Strut 3F with Three Loading Blocks

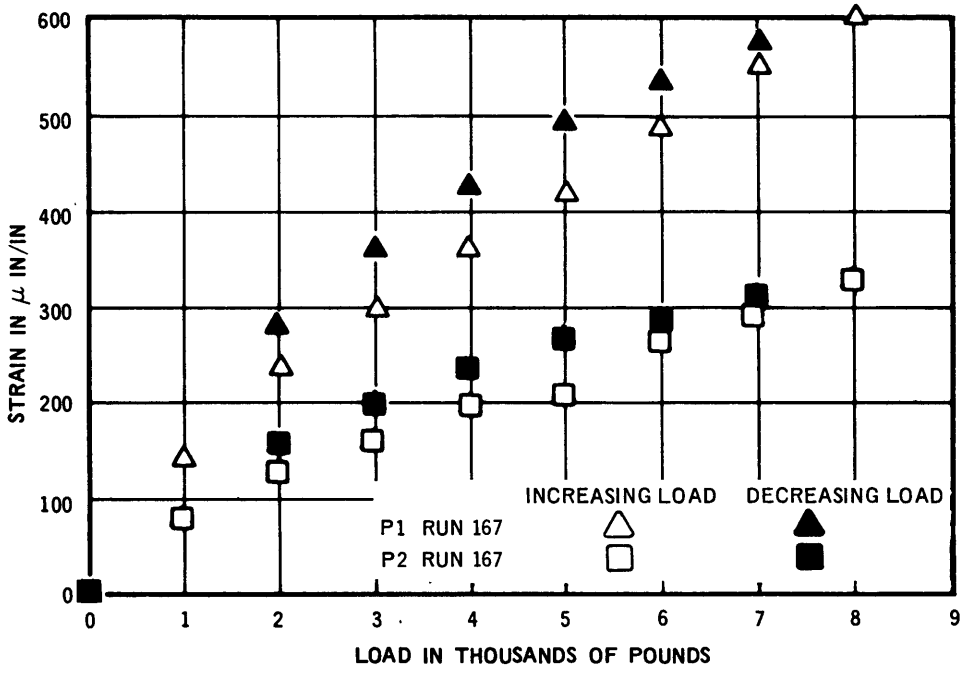

Figure 9a – Gages P1 and P2

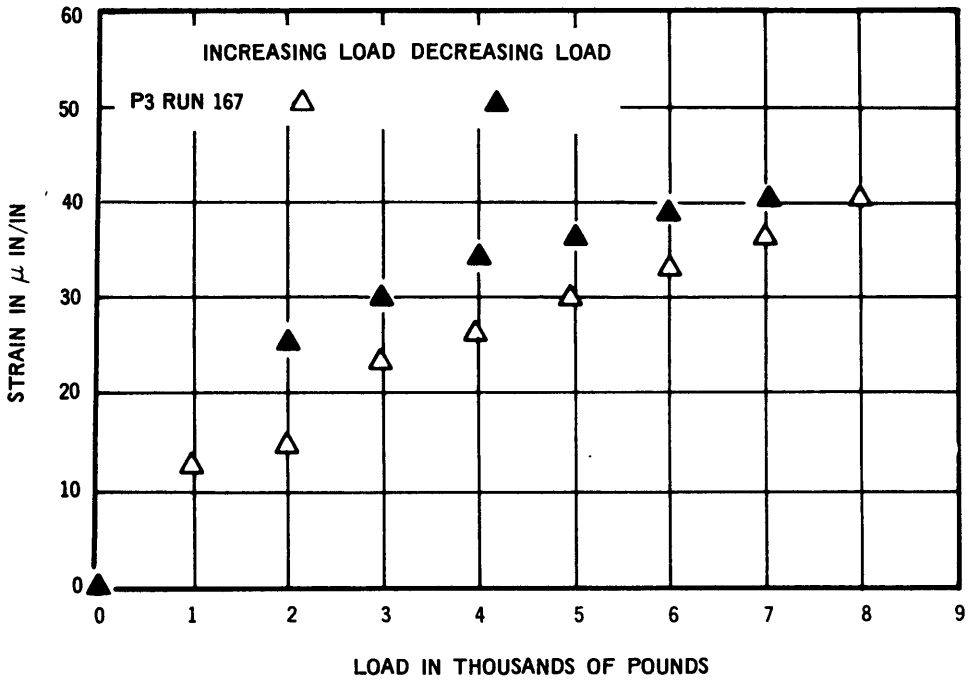

Figure 9b – Gage P3

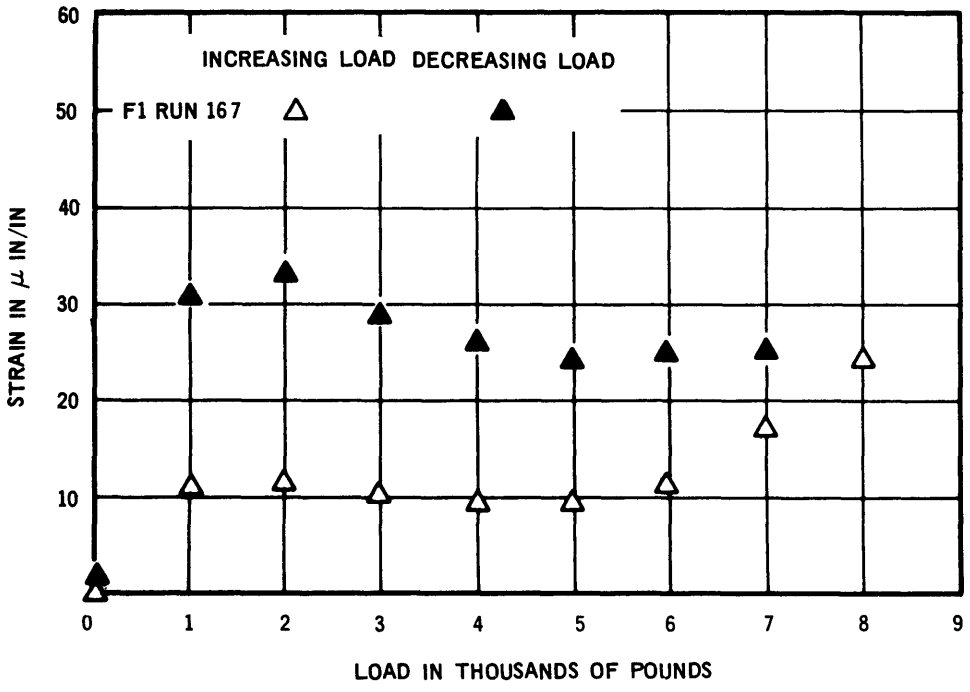

Figure 9c – Gage F1

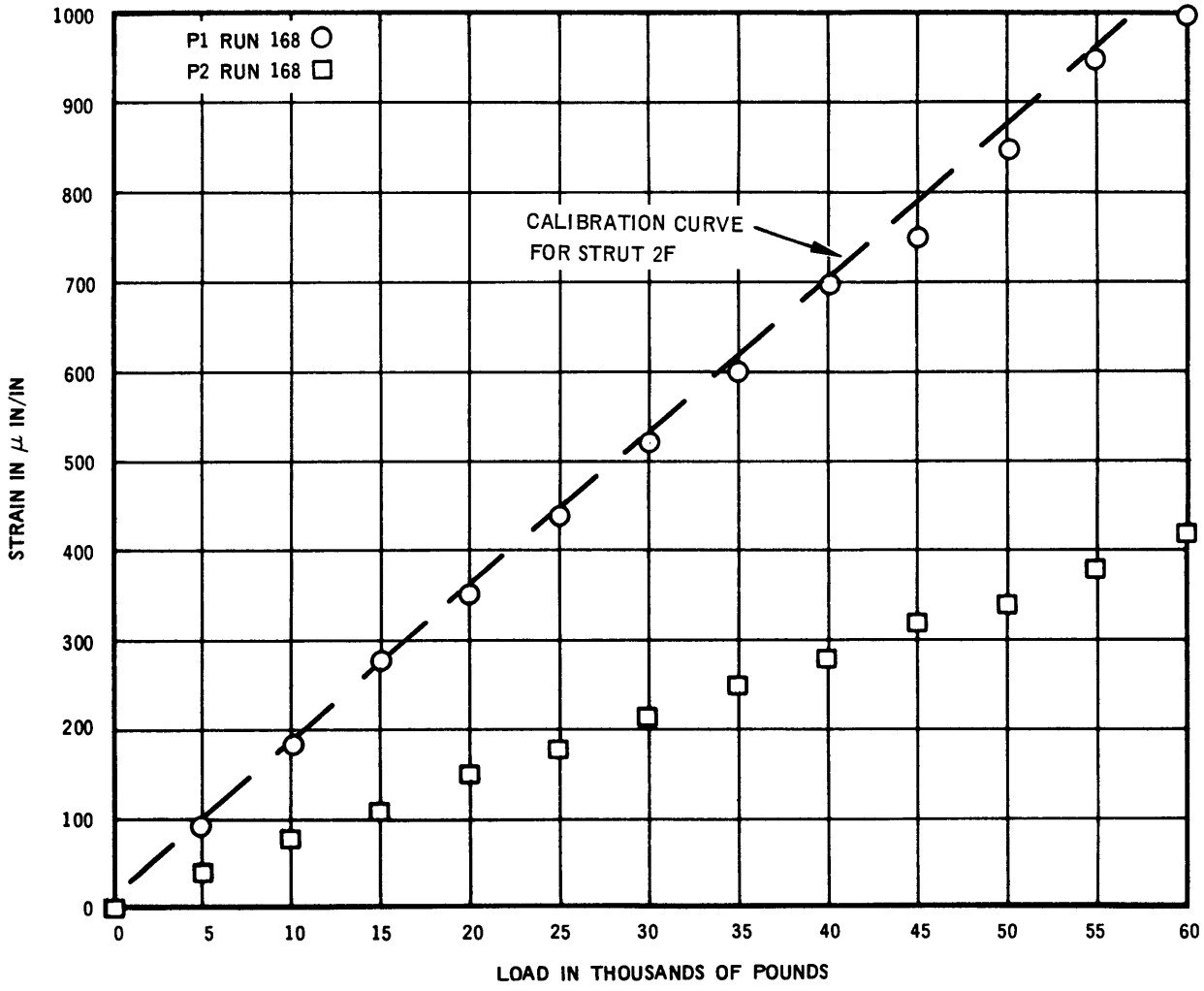

Figure 10 - Strain on Strut Skin versus Load for Strut 2F with One Loading Block

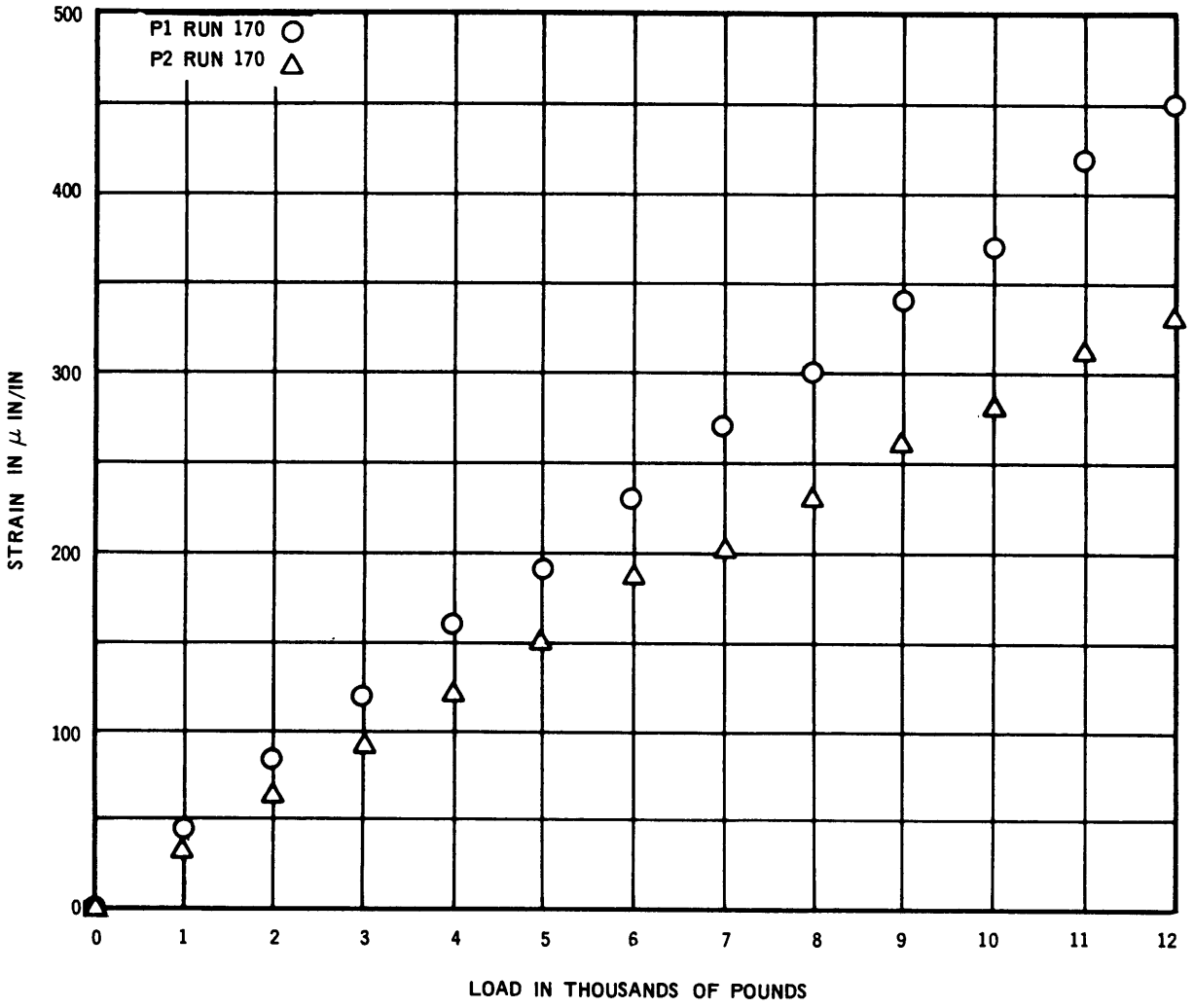

Figure 11 - Strain on Strut Skin versus Load for Strut 2F End Section Test with One Loading Block

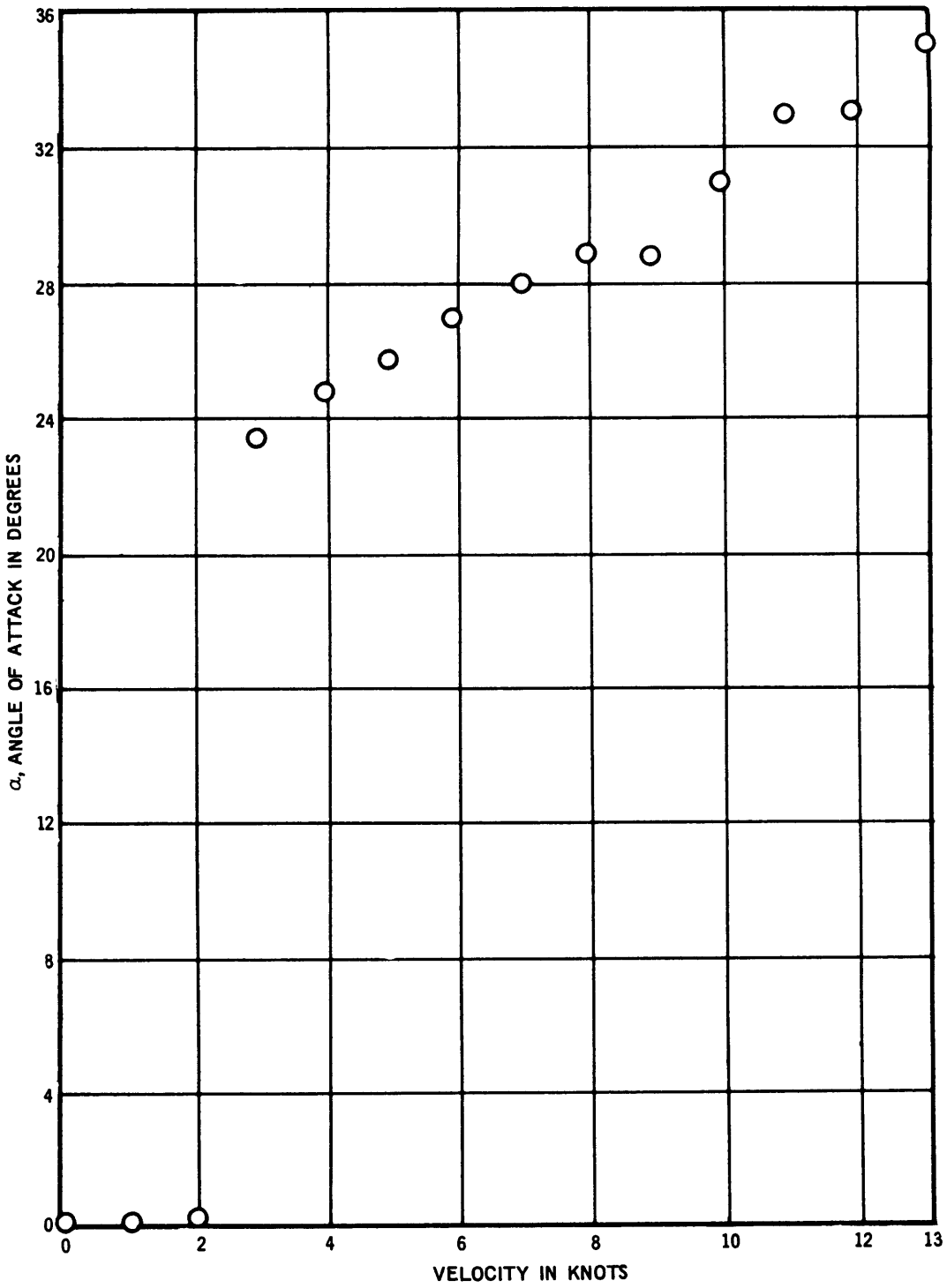

Figure 12 - Stable Angle of Attack for Rotating Strut 3R versus Velocity

Figure 13 - Accelerations versus Velocity for the Rotating Struts

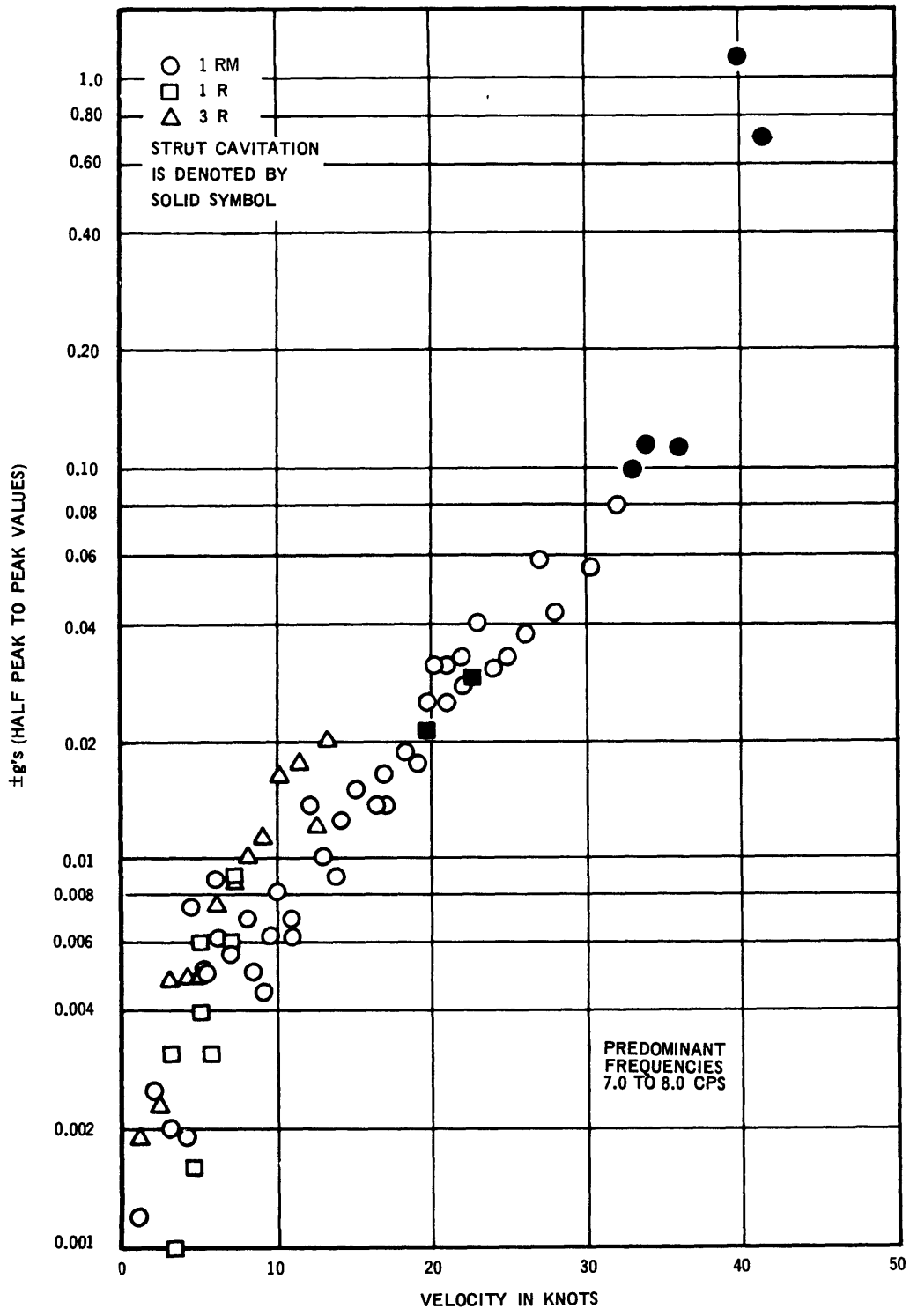

Figure 13a – Vertical Acceleration

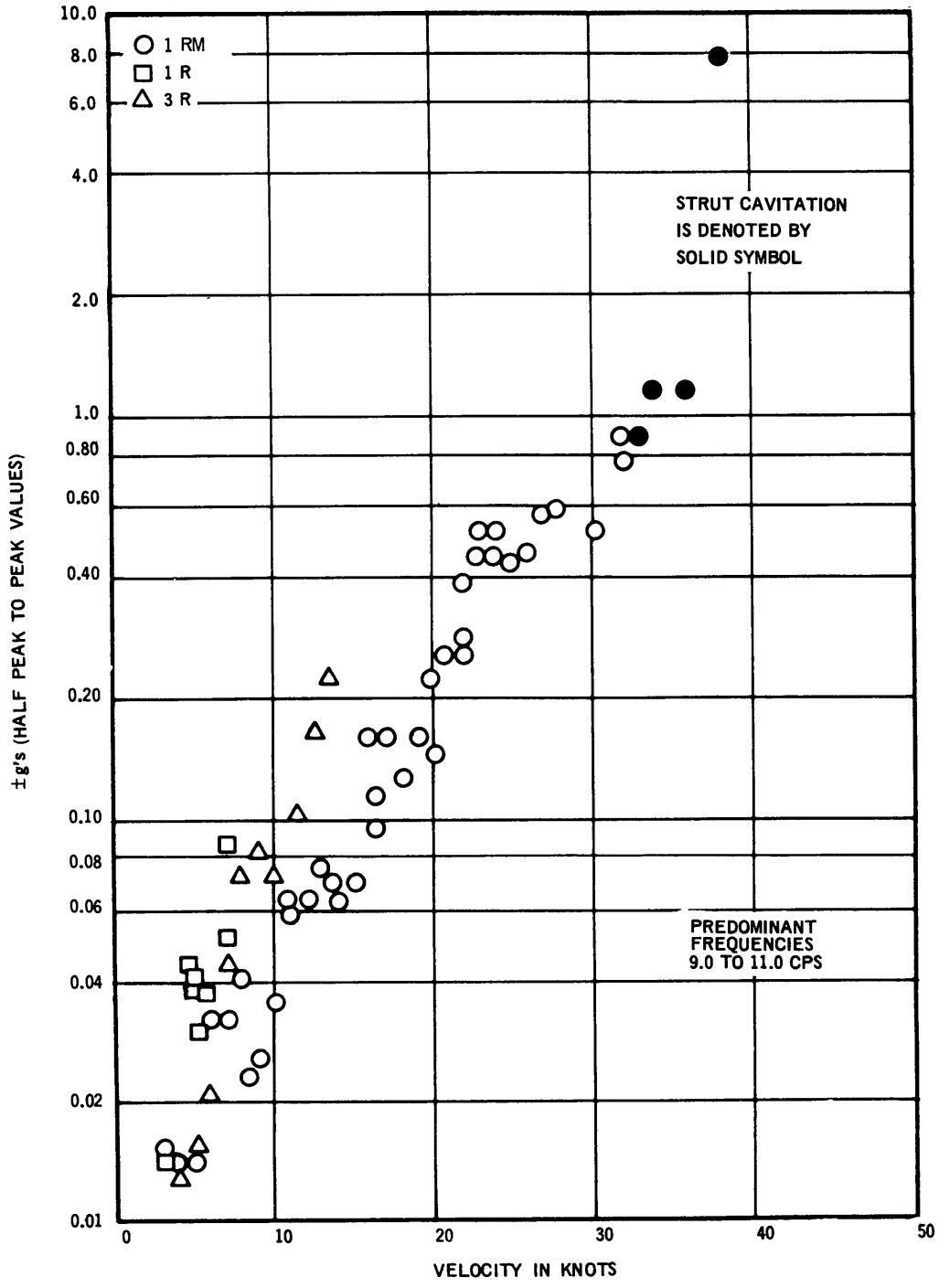

Figure 13b — Port-Starboard Acceleration

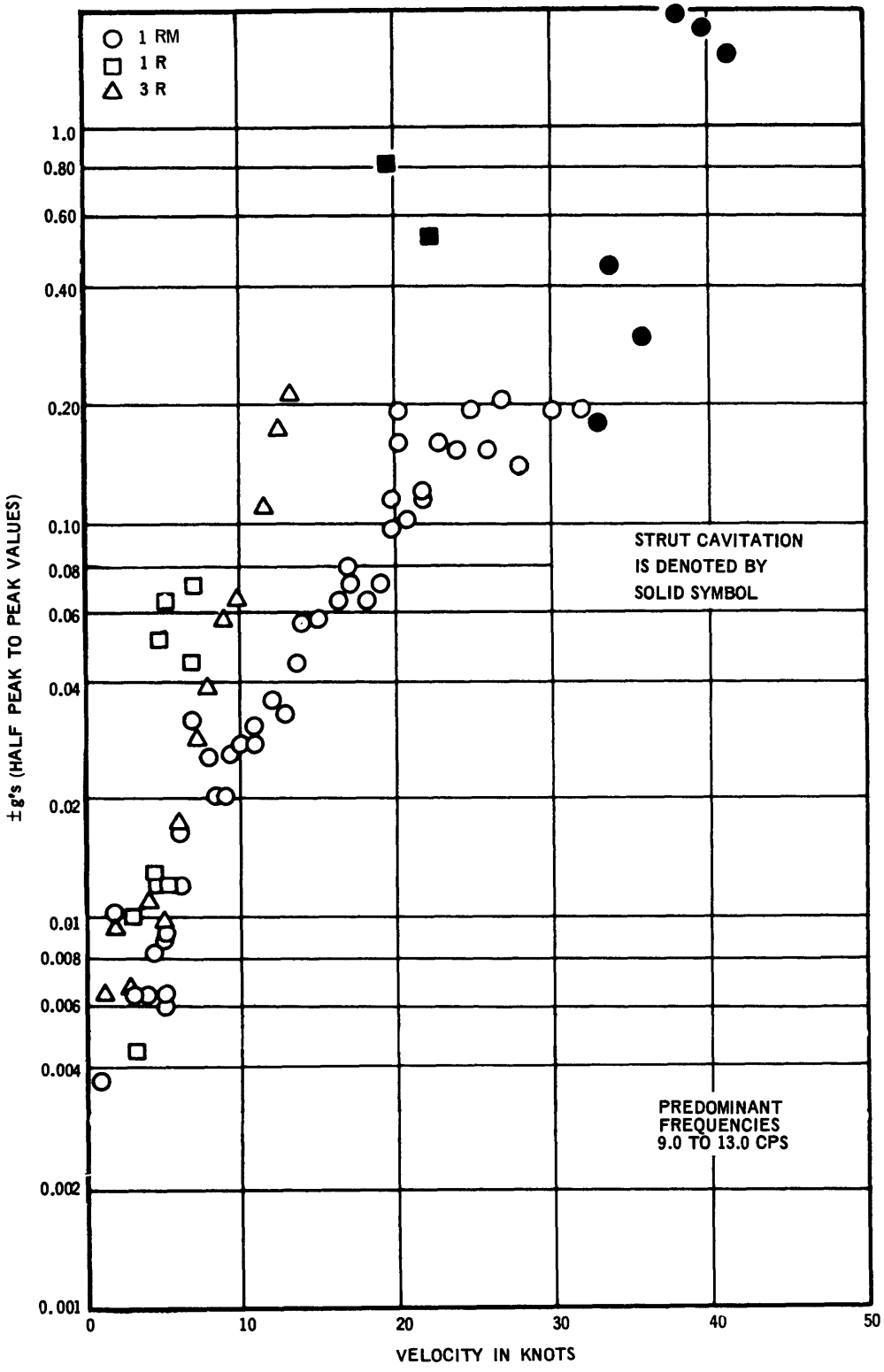

Figure 13c — Forward-Aft Acceleration

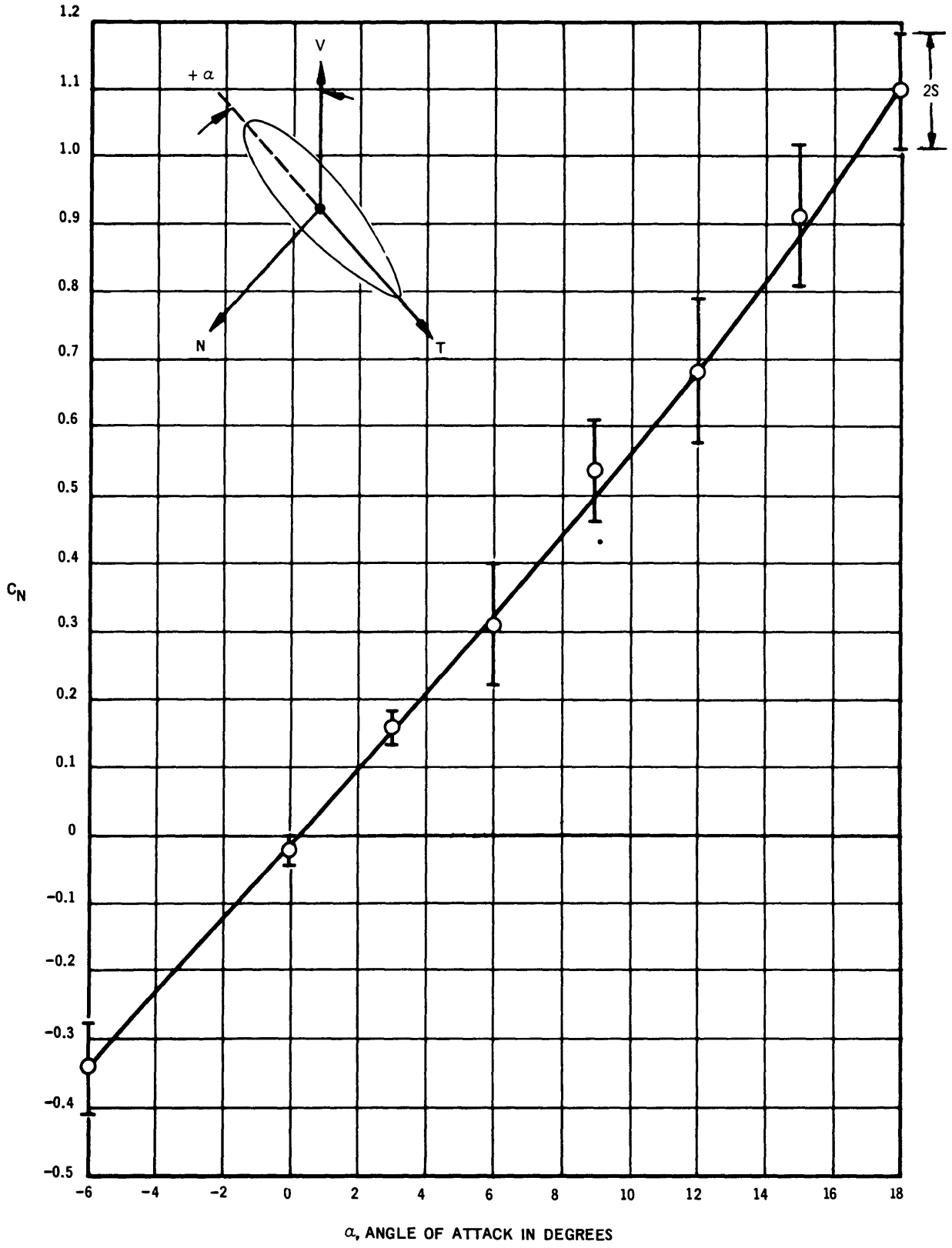

Figure 14 - Steady Normal Force Coefficient versus Angle of Attack for Strut 2F

Figure 15 - Steady Force Coefficients versus Angle of Attack for Strut 3F

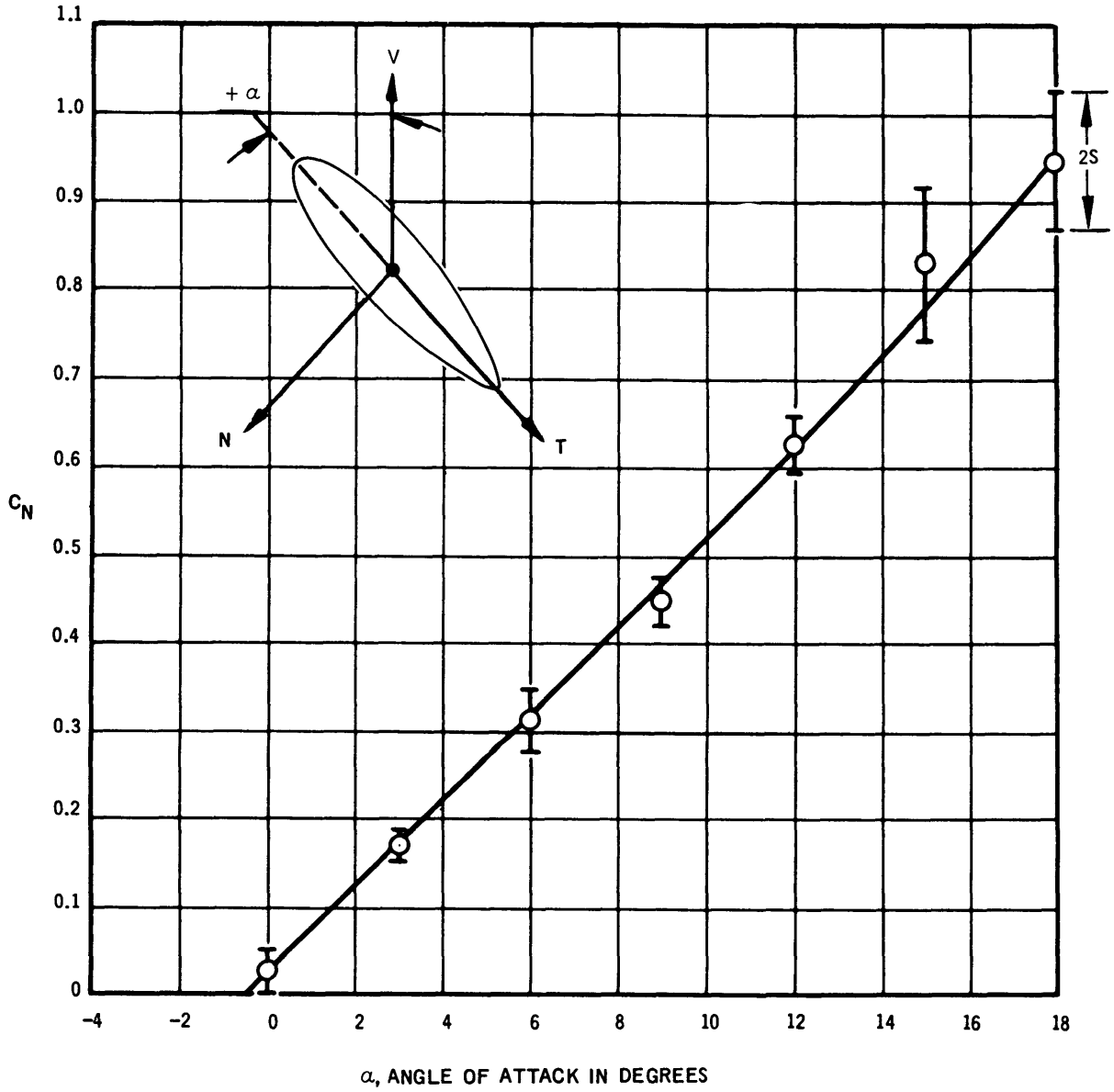

Figure 15a – Steady Normal Force Coefficient for Strut 3F

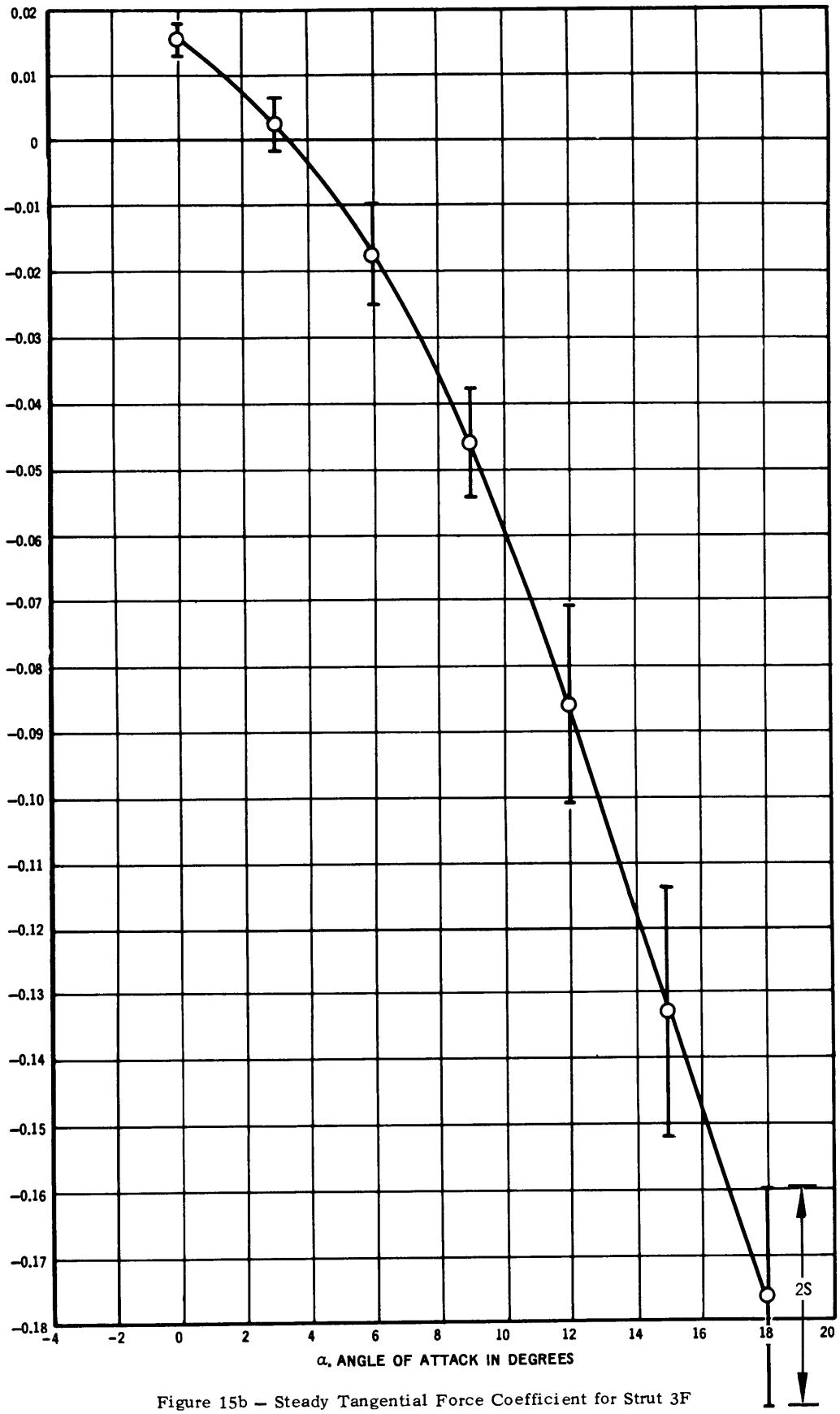

Figure 15b — Steady Tangential Force Coefficient for Strut 3F

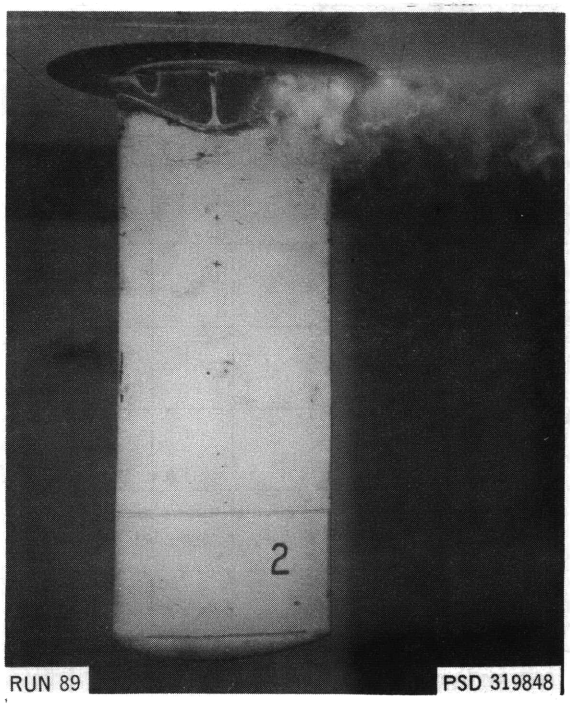

Figure 16a – "Root Cavitation at an Angle of Attack of 3 Degrees and a Velocity of about 32 Knots

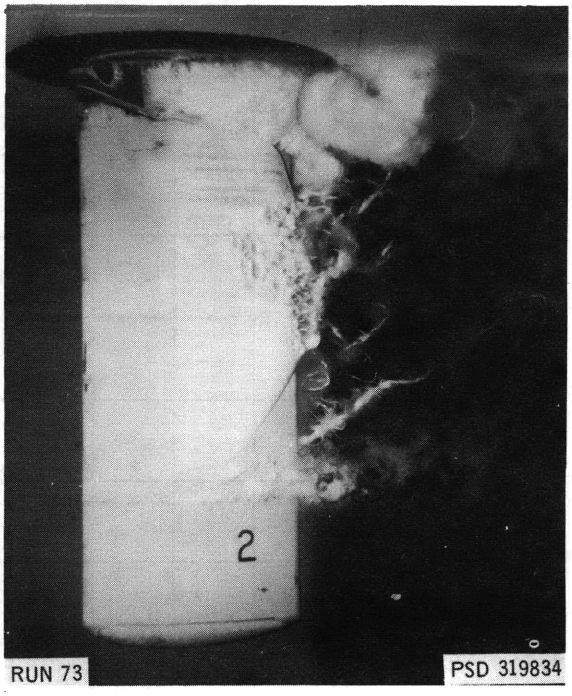

Figure 16b – "Root" Forward and "Strut" Cavitation at an Angle of Attack of 0 Degrees and a Velocity of about 35 Knots

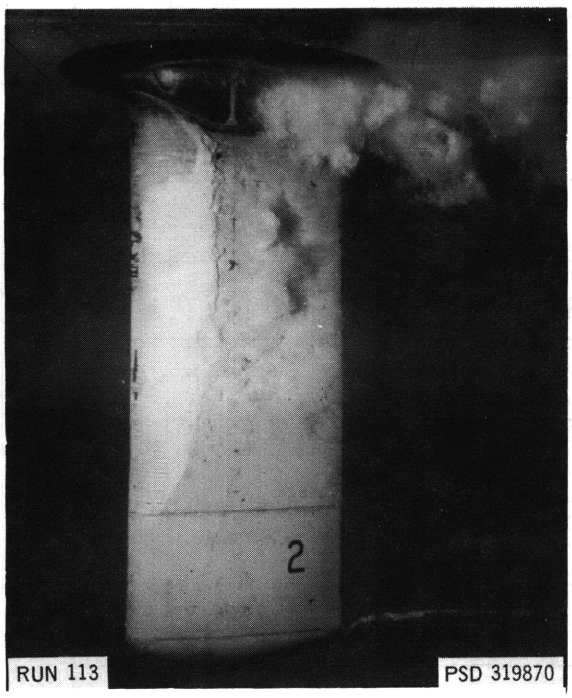

Figure 16c – "Root," "Strut," and "Tip Vortex" Cavitation at an Angle of Attack of 12 Degrees and a Velocity of about 23 Knots

Figure 16 – Sample Cavitation on Strut 2F

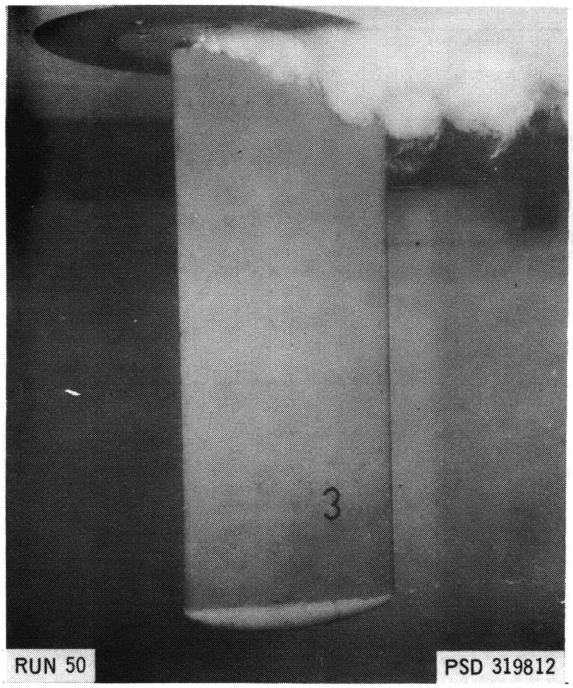

Figure 17a – "Root" Cavitation at an Angle of Attack of 12 Degrees and a Velocity of about 17.5 Knots

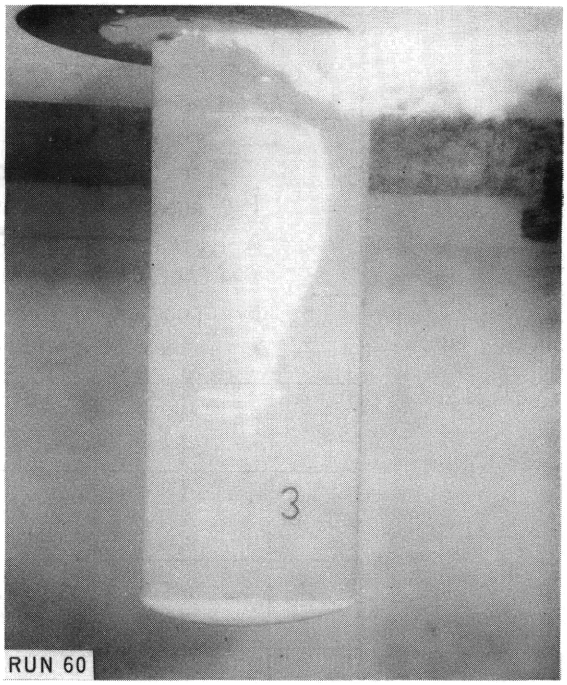

Figure 17b – "Root" and "Strut" Cavitation at an Angle of Attack of 0 Degrees and a Velocity of about 37 Knots

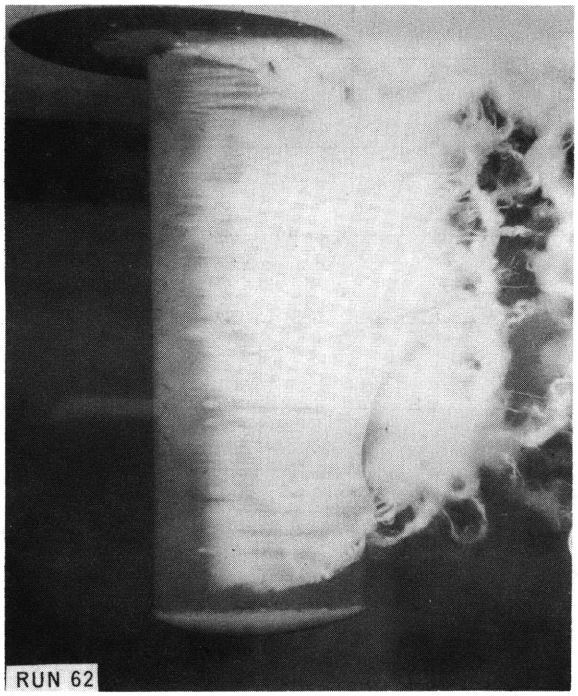

Figure 17c – "Root" and "Strut" Cavitation United in a "Full" Cavity at an Angle of Attack of 0 Degrees and a Velocity of About 44.5 Knots

Figure 17 – Sample Cavitation on Strut 3F

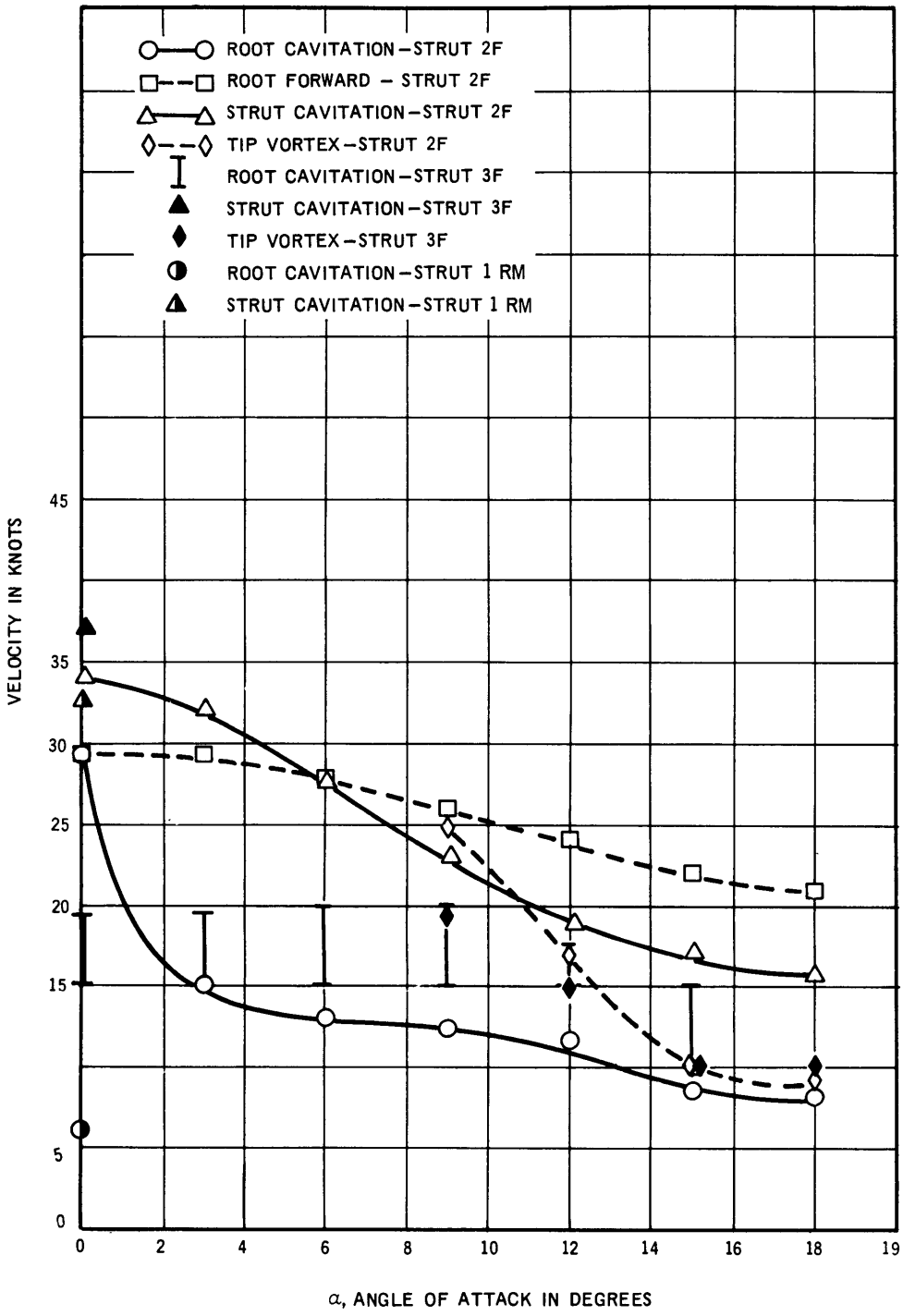

Figure 18 - Summary of Cavitation Inception Velocities versus Angle of Attack for the Test Depth of 1.0 Foot

Figure 19 - Unsteady Normal Force Coefficient versus Velocity for Strut 2F

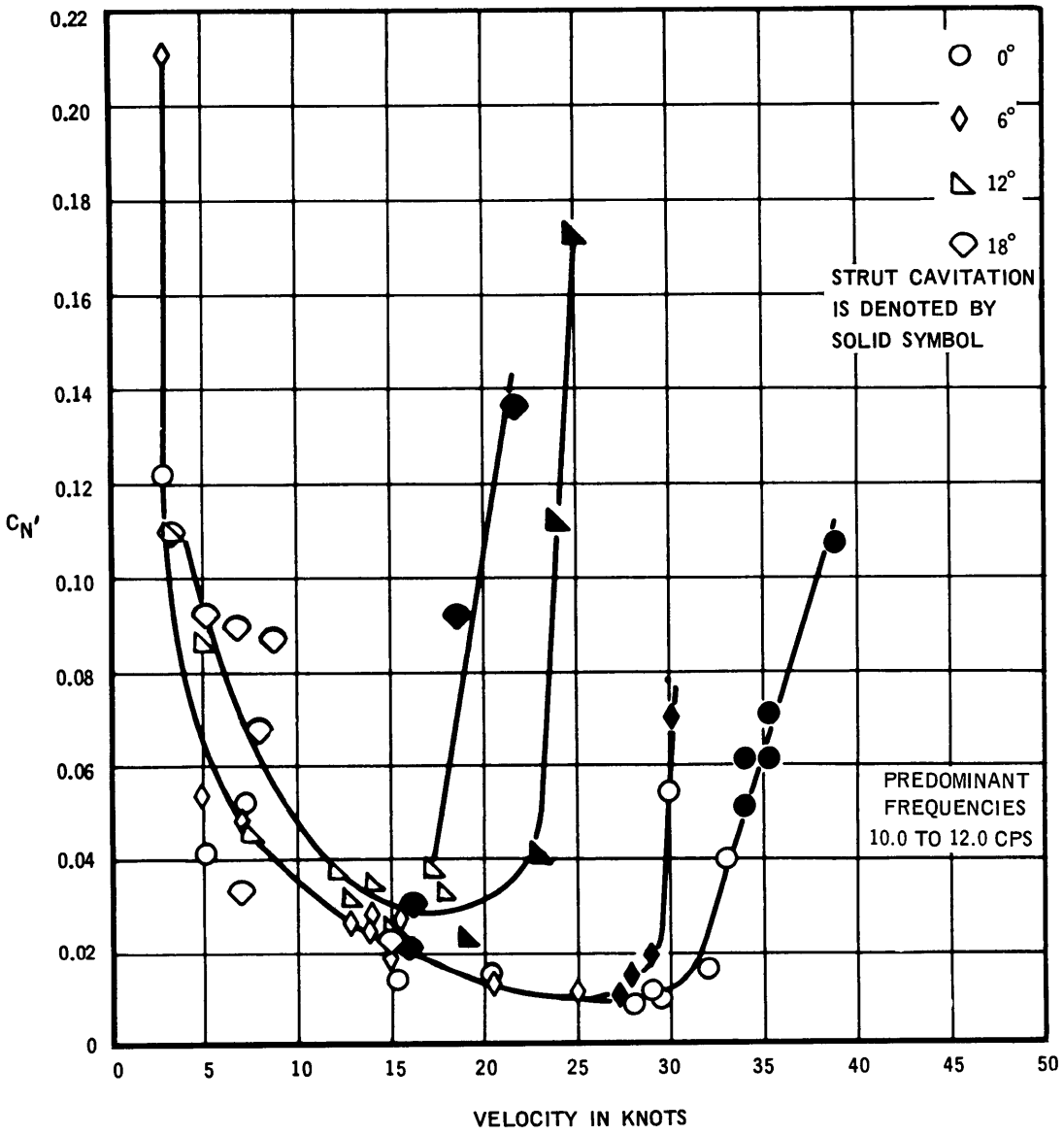

Figure 19a – Angles of Attack of 0, 6, 12, and 18 Degrees

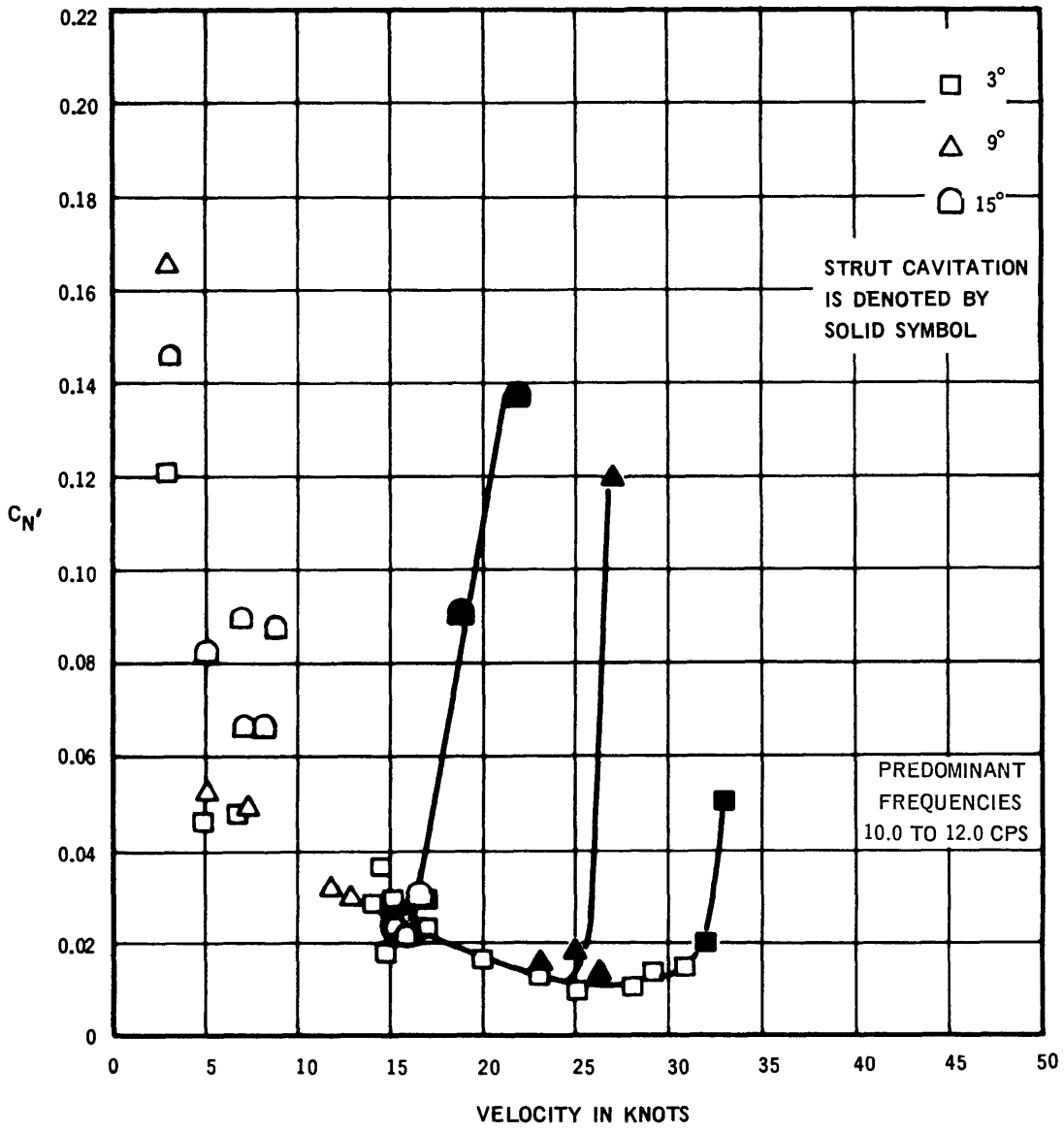

Figure 19b – Angles of Attack of 3, 9, and 15 Degrees

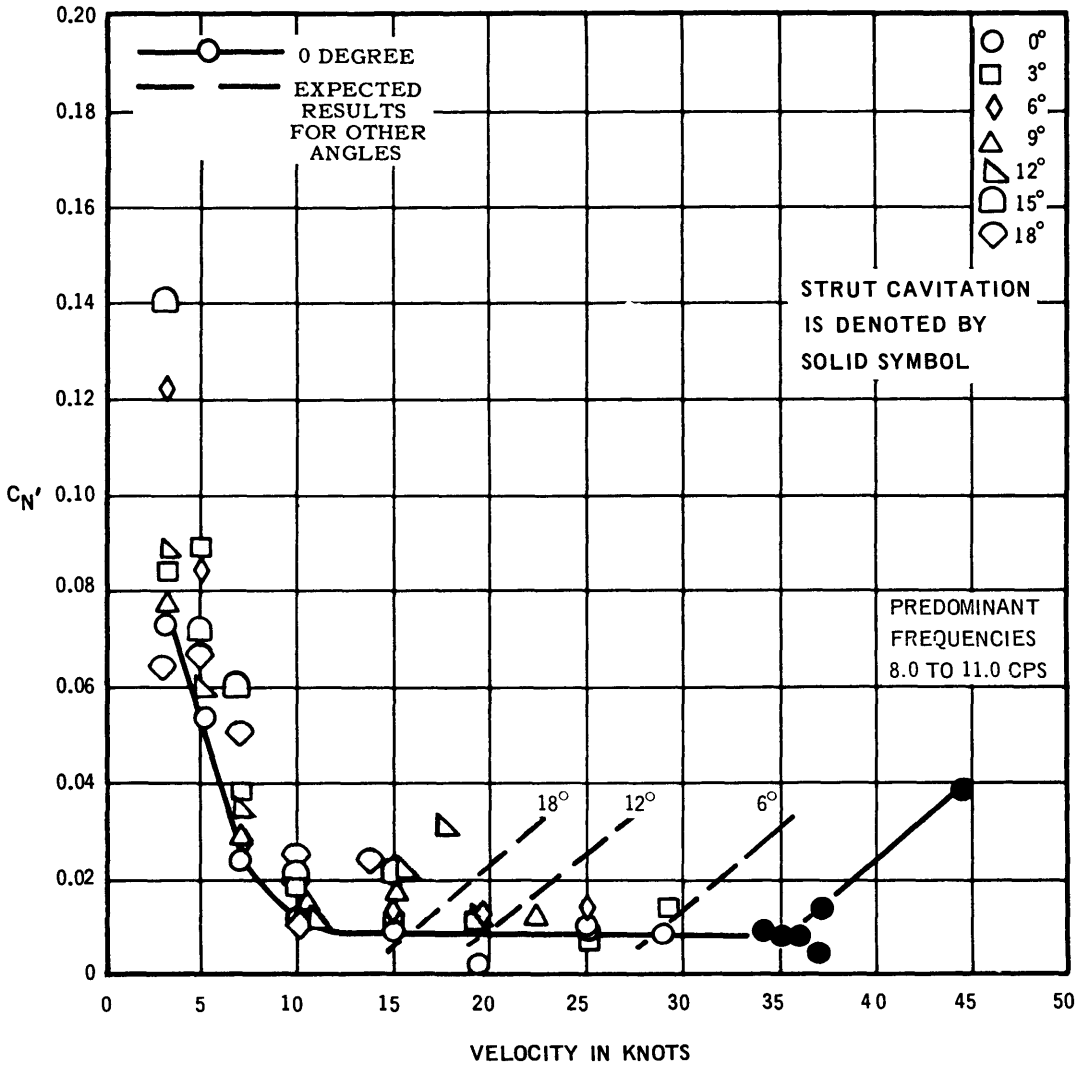

Figure 20 - Unsteady Normal Force Coefficient versus Velocity for Strut 3F

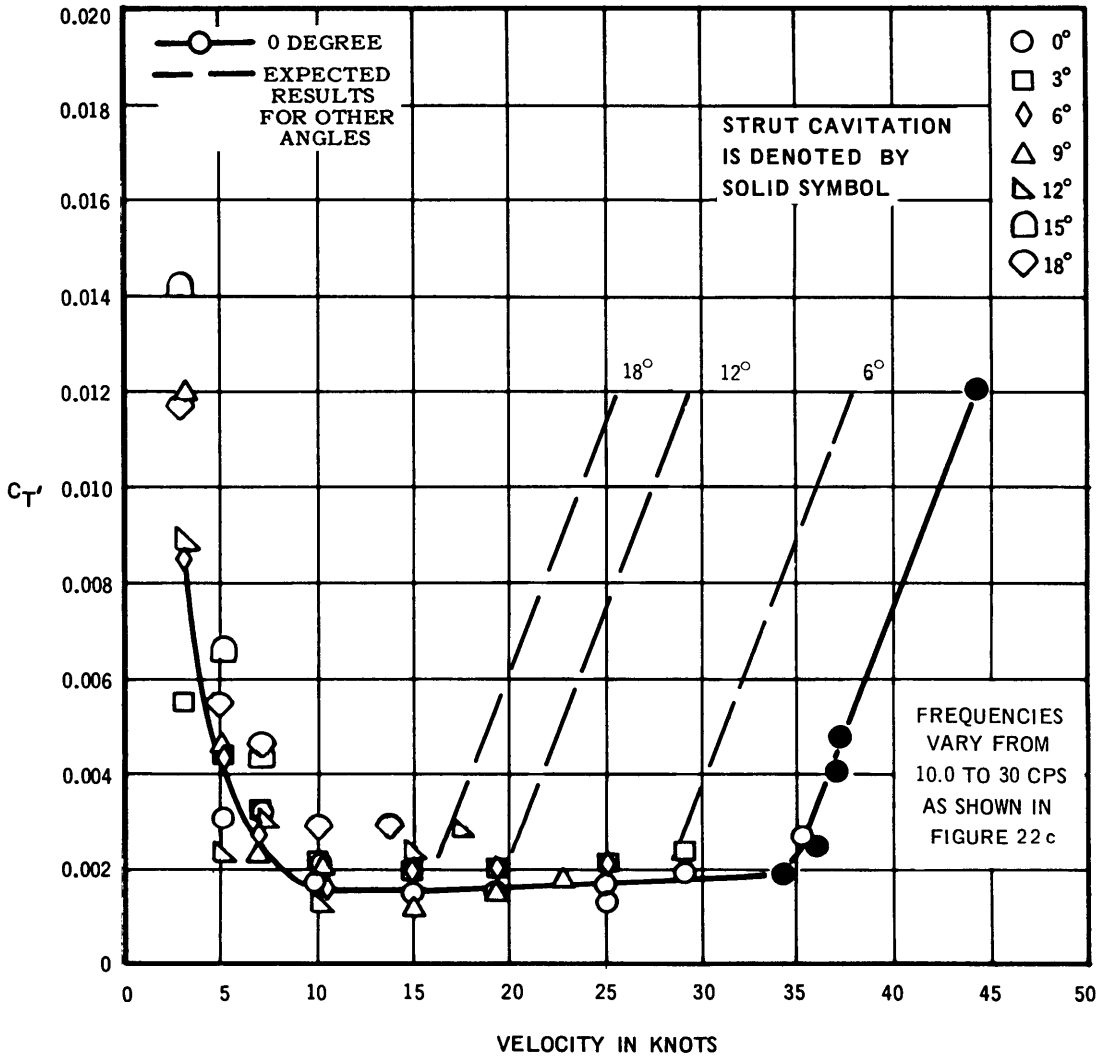

Figure 21 - Unsteady Tangential Force Coefficient versus Velocity for Strut 3F

Figure 22 - Accelerations versus Velocity for Strut 3F

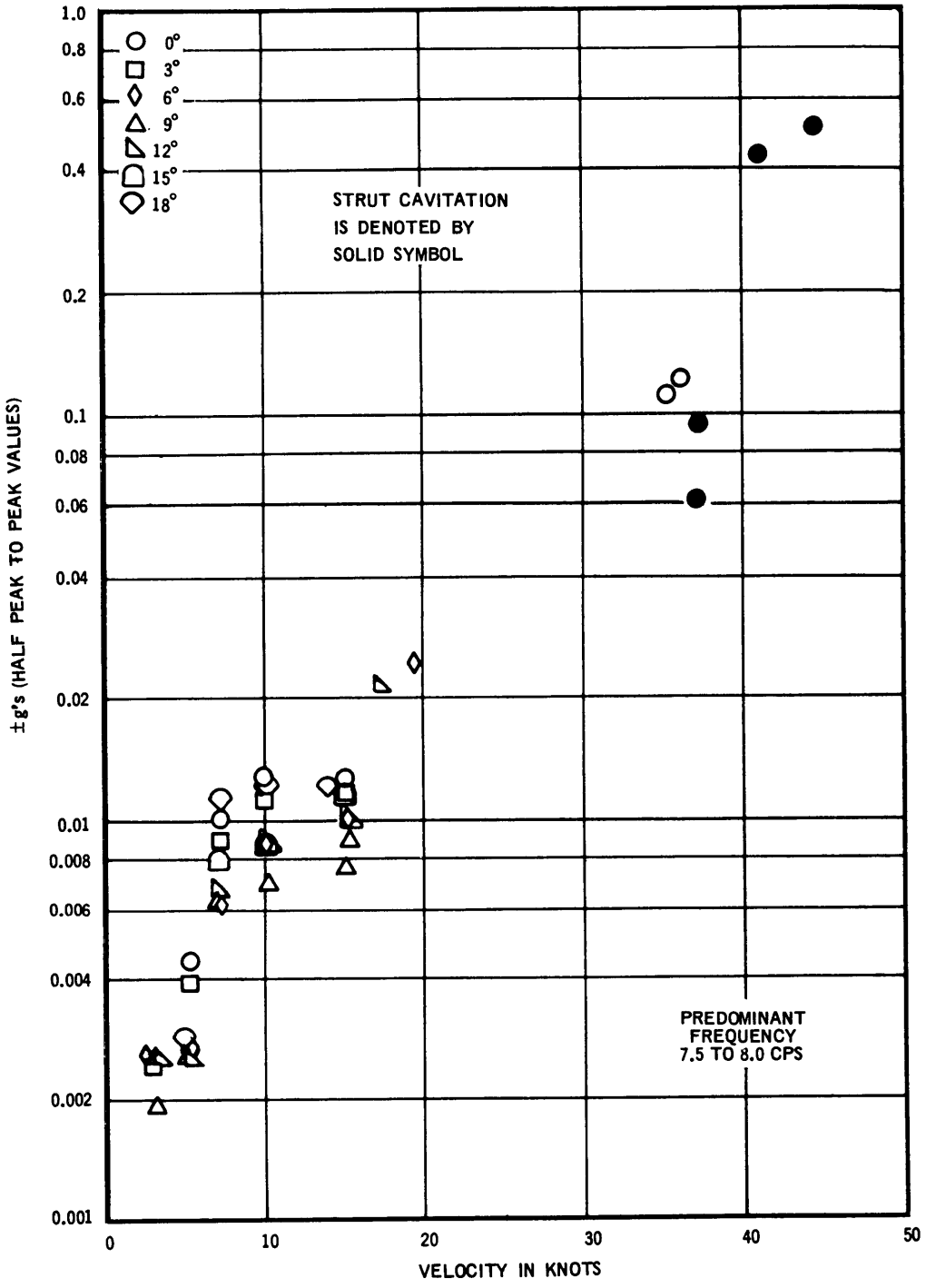

Figure 22a – Vertical Acceleration

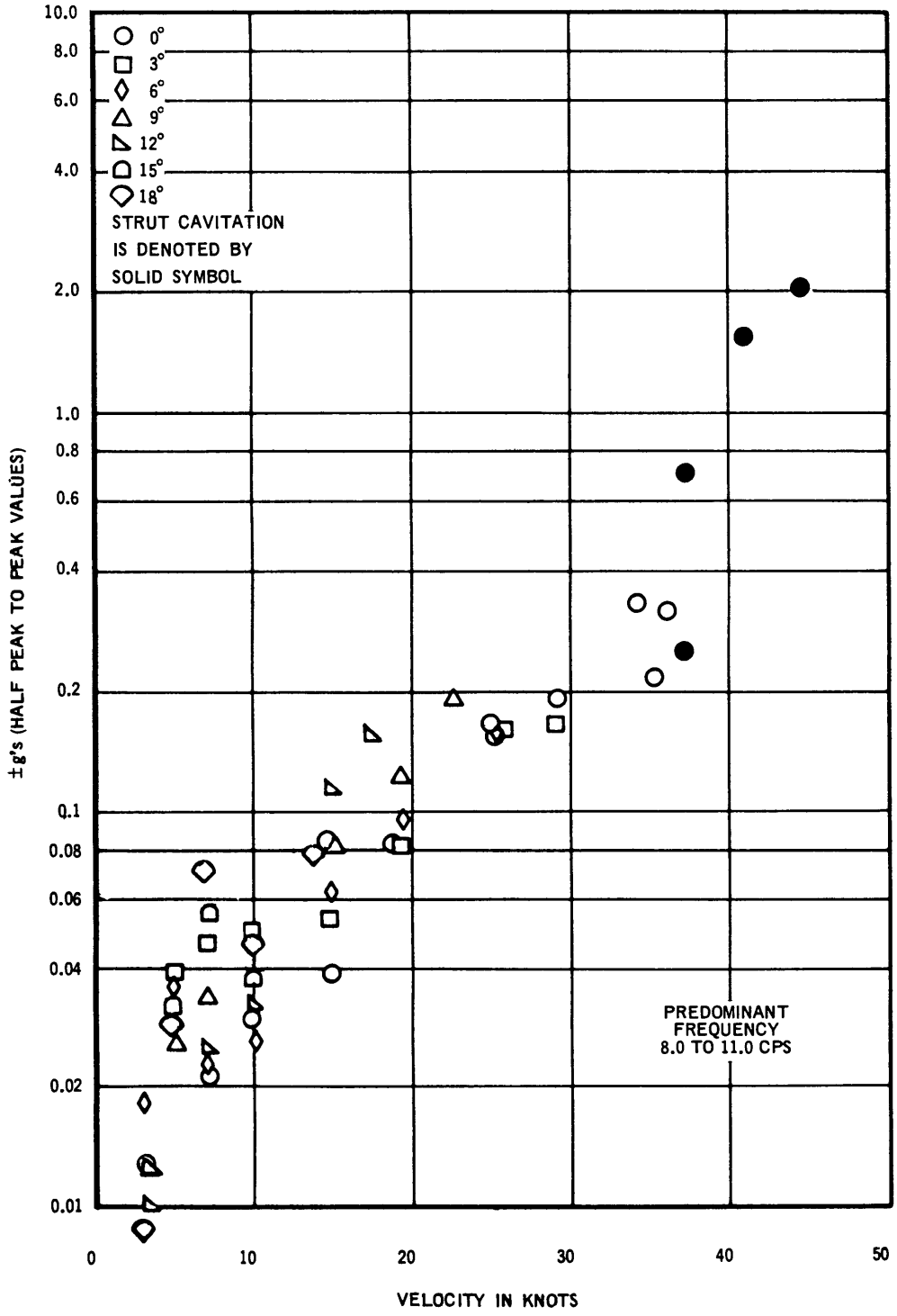

Figure 22b – Port-Starboard Acceleration

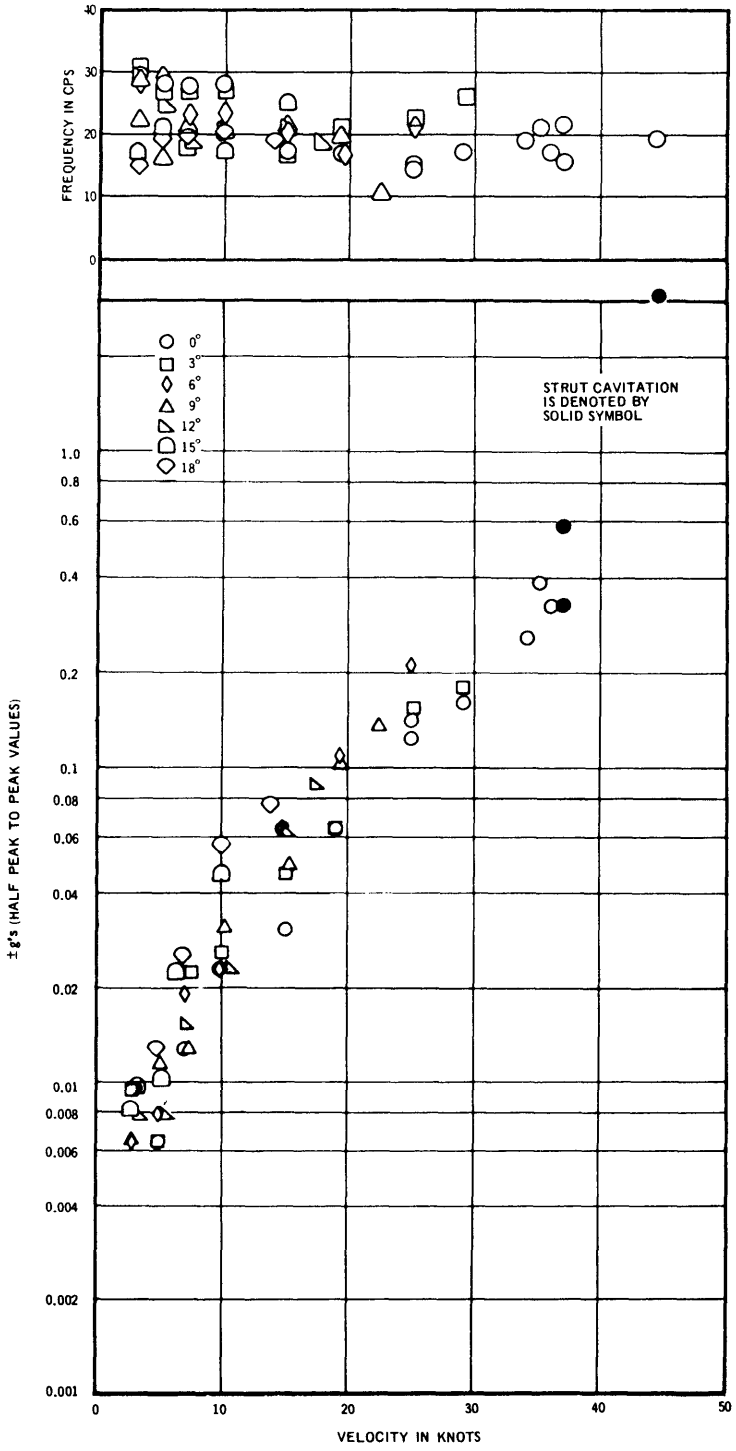

Figure 22c – Forward-Aft Acceleration

Figure 23 - Acceleration Coefficients versus Velocity for Strut 3F

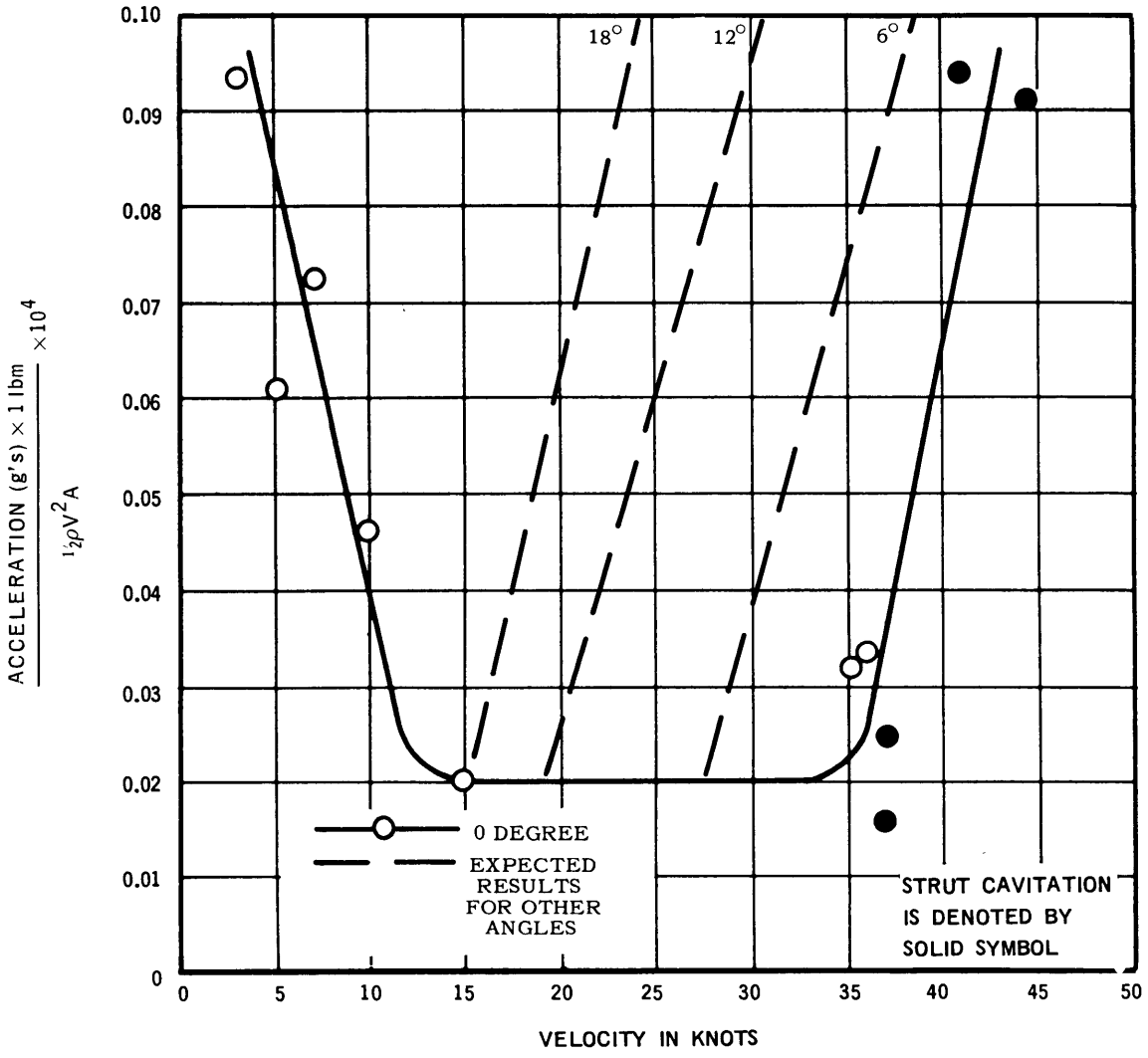

Figure 23a — Vertical Acceleration Coefficient

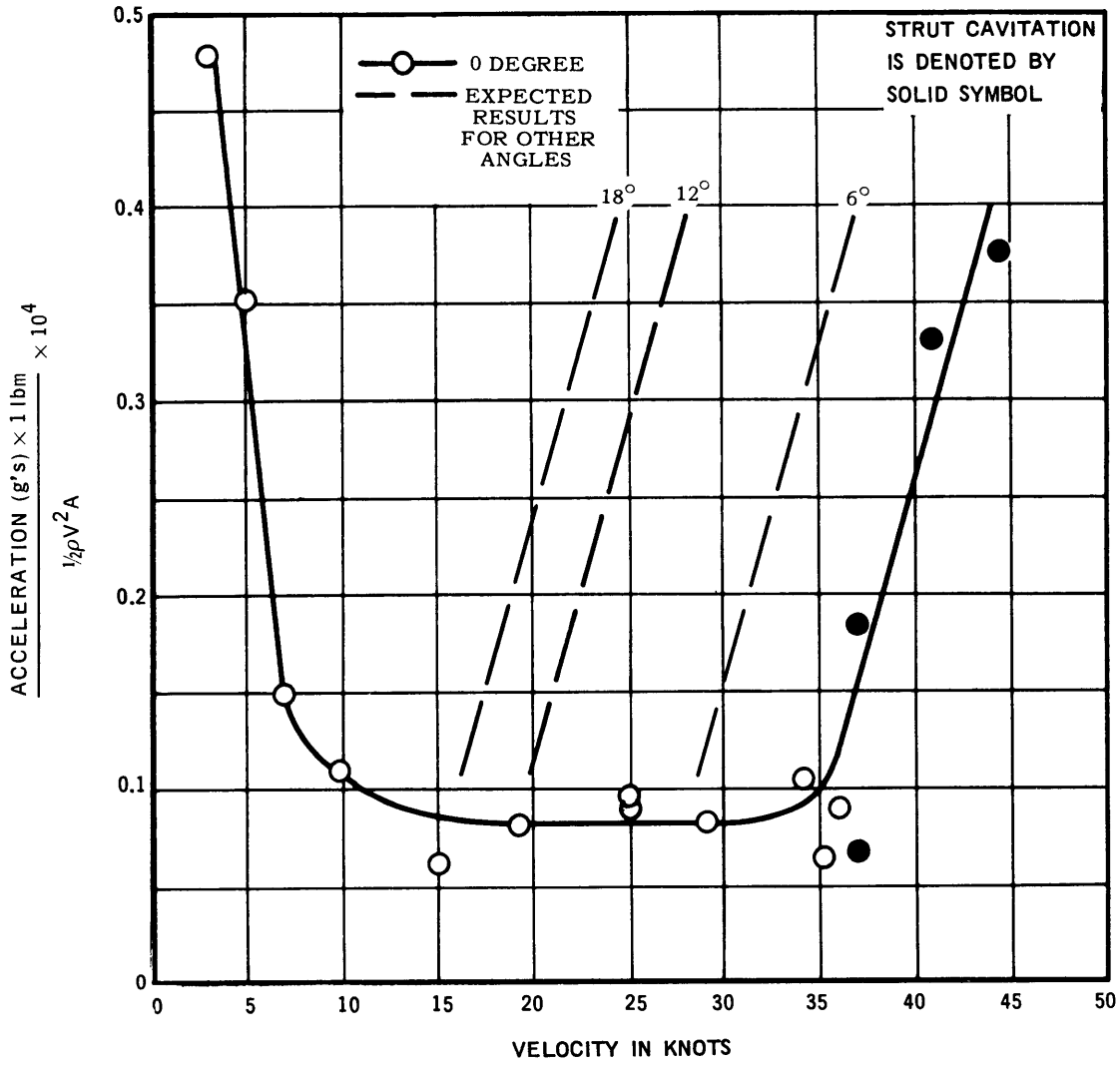

Figure 23b — Port-Starboard Acceleration Coefficient

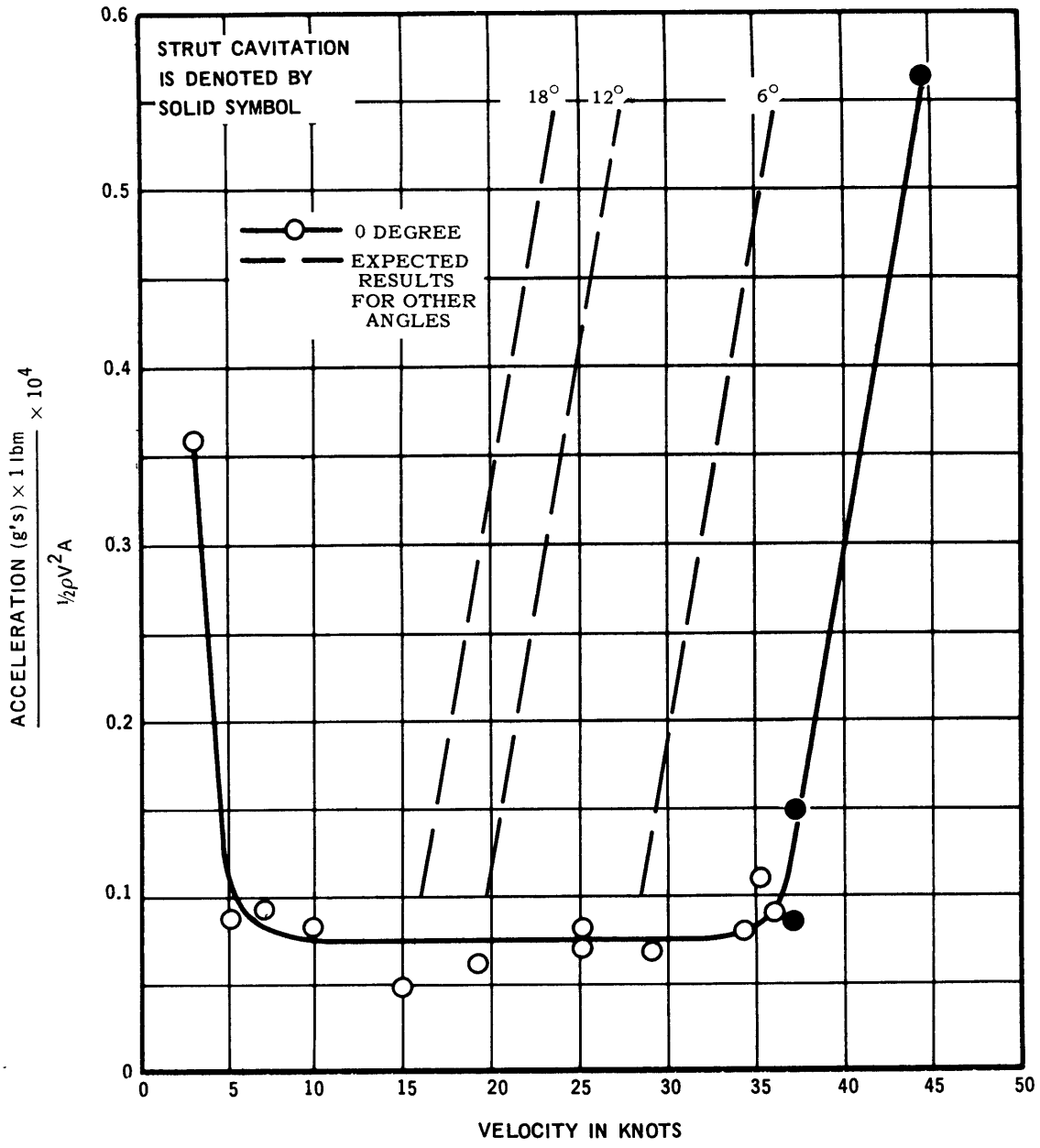

Figure 23c – Forward-Aft Acceleration Coefficient

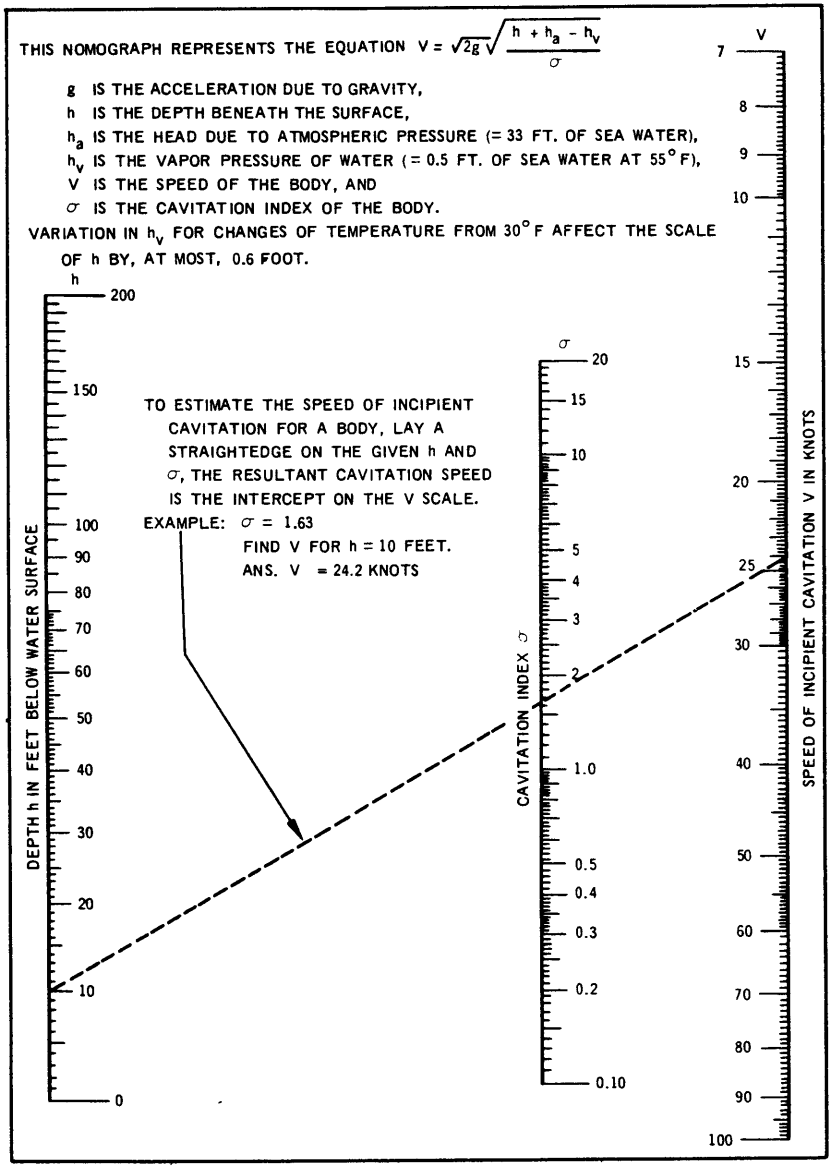

Figure 24 - Cavitation Nomograph

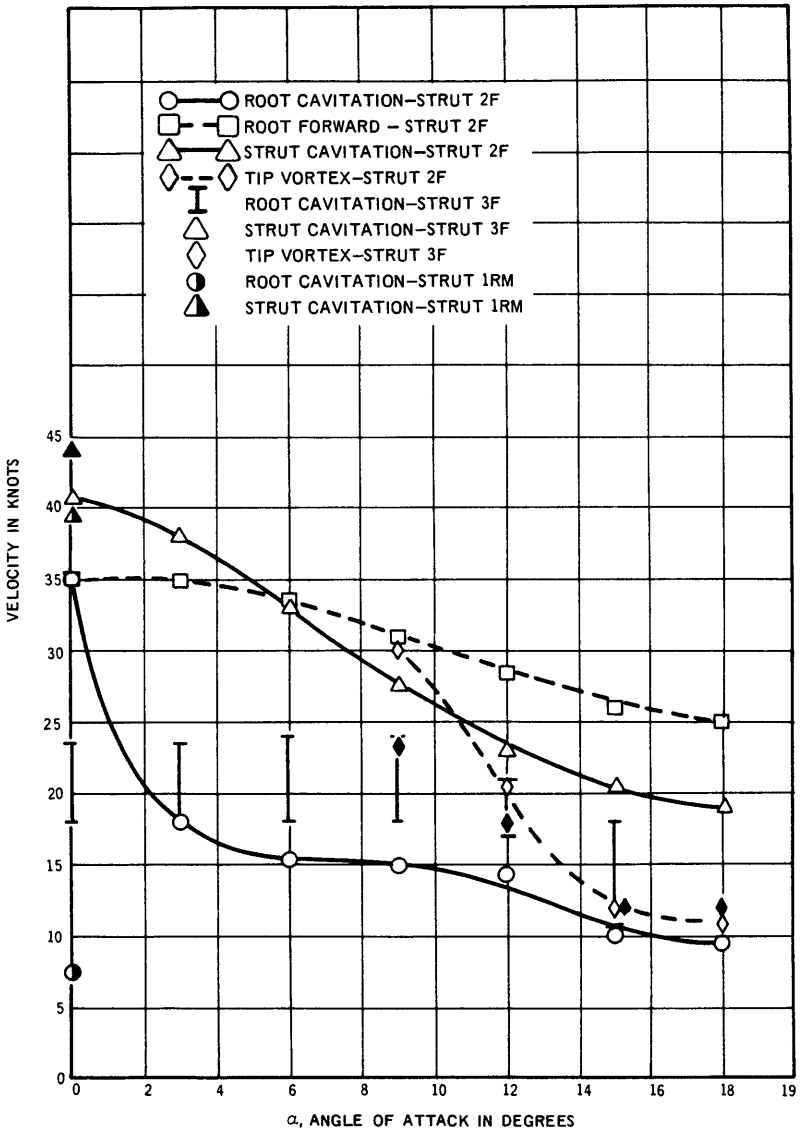

Figure 25 - Summary of Cavitation Inception Velocities versus Angle of Attack for a Depth of 15 Feet

TABLE 1

Physical Characteristics of the TRG Hydrophone Struts

NAME & CODE OF STRUT	AXIS OF ROTATION	BEARING FRICTION TORQUE	SKIN– THICKNESS, MATERIAL, YIELD POINT	END SECTION– THICKNESS, MATERIAL	METHOD OF SKIN ATTACHMENT	BASE PLATE– THICKNESS, MATERIAL, YIELD POINT	SHAFT– MATERIAL, YIELD POINT	INFORMATION MONITORED DURING TEST*
ROTATING STRUT 1R	18% CHORD	30 ft lb	11 GAUGE (0.119 in) MILD STEEL Y_p = 35 ksi		WELDED	3 inch MILD STEEL Y_p = 35 ksi	MILD STEEL Y_p = 35 ksi	LVDT SGP ACC HYD
ROTATING STRUT MODIFIED 1RM	12% CHORD (based on 3 ft Chord)	6 ft lb						LVDT ACC HYD
FIXED STRUT 2F			3/8 inch 4130 STEEL Y_p = 60 ksi	14 GAUGE TYPE 316 STAINLESS STEEL SHEET	WELDED	3 inch 4130 STEEL Y_p = 60 ksi		SGP ACC HYD
ROTATING STRUT 3F			11 GAUGE (0.119 in) MILD STEEL Y_p = 35 ksi		SCREWED	2 inch 4130 STEEL Y_p = 60 ksi	4130 STEEL Y_p = 60 ksi	SGF SGP ACC HYD
ROTATING STRUT 3R	18% CHORD	3 ft lb						LVDT SGF SGP ACC, HYD

*LVDT = Linear variable differential transformer used for angle of attack measurement.
SGP = Strain gages in port-starboard direction.
SGF = Strain gages in forward-aft direction.
ACC = Accelerometers in bottom of strut.
HYD = Hydrophone in bottom of strut.

TABLE 2

Deflections of Strut 3F versus Load with One Loading Block

LOAD ($lb \times 10^{-3}$)	Indicator Number – Actual and Corrected Displacement in Inches											
	1		2		3		4		5		6	
0	0.000	0.000	0.000	0.000	0.000	0.000	0.000	0.000	0.000	0.000	0.000	0.000
1	0.034	0.034	0.094	0.094	0.051	0.051	-0.007	-0.007	0.044	0.044	0.096	0.096
2	0.051	0.050	0.175	0.169	0.172	0.160	-0.004	-0.005	0.094	0.088	0.191	0.179
3	0.070	0.068	0.245	0.226	0.292	0.256	-0.005	-0.008	0.142	0.123	0.286	0.250
4	0.098	0.094	0.317	0.288	0.321	0.268	-0.004	-0.008	0.186	0.157	0.375	0.321
5	0.129	0.125	0.396	0.361	0.546	0.481	-0.010	-0.015	0.225	0.190	0.454	0.387
6	0.151	0.146	0.464	0.422	0.656	0.579	-0.011	-0.017	0.270	0.228	0.538	0.459
7	0.163	0.157	0.517	0.466	0.748	0.653	-0.017	-0.024	0.311	0.260	0.617	0.520
8	0.175	0.168	0.573	0.519	0.841	0.740	-0.019	-0.027	0.354	0.300	0.697	0.594
9	0.188		0.626		0.932		-0.018		0.392		0.770	
8	0.185	0.178	0.594	0.540	0.875	0.774	-0.019	-0.027	0.367	0.313	0.712	0.609
7	0.181	0.174	0.550	0.496	0.798	0.697	-0.020	-0.028	0.320	0.266	0.639	0.536
6	0.175	0.168	0.503	0.449	0.710	0.609	-0.020	-0.028	0.279	0.225	0.560	0.457
5	0.169	0.163	0.456	0.402	0.627	0.544	-0.020	-0.027	0.237	0.192	0.485	0.400
4	0.160	0.154	0.402	0.357	0.537	0.454	-0.021	-0.028	0.194	0.149	0.402	0.317
3	0.148	0.142	0.340	0.295	0.327	0.254	-0.022	-0.029	0.148	0.103	0.314	0.229
2	0.130	0.125	0.270	0.240	0.212	0.152	-0.020	-0.025	0.102	0.072	0.223	0.163
1	0.106	0.103	0.189	0.169	0.180	0.140	-0.016	-0.019	0.054	0.034	0.124	0.094
0	0.066	0.066	0.074	0.074	0.010	0.010	-0.007	-0.007	0.003	0.003	0.012	0.012

TABLE 3

Deflections of Strut 3F with Three Loading Blocks

LOAD (lbs × 10^{-3})	Indicator Number – Actual and Corrected Displacement in Inches																	
	1		2		3		4		5		6		7		8		9	
0	0.000	0.000	0.000	0.000	0.000	0.000	0.000	0.000	0.000	0.000	0.000	0.000	0.000		0.000		0.000	
1	0.036	0.036	0.096	0.093	0.157	0.151	-0.009	-0.009	0.039	0.036	0.096	0.090	-0.001		-0.001		0.000	
2	0.057	0.056	0.155	0.145	0.254	0.136	-0.011	-0.012	0.072	0.062	0.157	0.139	-0.002		-0.003		-0.004	
3	0.073	0.071	0.197	0.181	0.320	0.290	-0.015	-0.017	0.094	0.078	0.201	0.171	-0.003		-0.005		-0.006	
4	0.087	0.085	0.238	0.219	0.387	0.351	-0.016	-0.019	0.116	0.097	0.245	0.209	-0.004		-0.006		-0.009	
5	0.098	0.095	0.273	0.251	0.434	0.393	-0.017	-0.020	0.136	0.114	0.284	0.242	-0.005		-0.007		-0.012	
6	0.110	0.107	0.308	0.282	0.505	0.458	-0.017	-0.021	0.156	0.130	0.324	0.276	-0.005		-0.008		-0.014	
7	0.121	0.117	0.344	0.312	0.563	0.504	-0.017	-0.022	0.176	0.144	0.363	0.303	-0.006		-0.010		-0.014	
8	0.136	0.131	0.383	0.345	0.624	0.553	-0.017	-0.023	0.199	0.161	0.407	0.434	-0.006		-0.012		-0.013	
7	0.131	0.126	0.365	0.327	0.590	0.519	-0.018	-0.024	0.184	0.146	0.380	0.307	-0.006		-0.012		-0.012	
6	0.124	0.119	0.342	0.304	0.548	0.477	-0.018	-0.024	0.171	0.133	0.353	0.280	-0.006		-0.012		-0.010	
5	0.115	0.110	0.312	0.274	0.502	0.431	-0.019	-0.025	0.149	0.111	0.317	0.244	-0.005		-0.012		-0.007	
4	0.105	0.100	0.280	0.242	0.452	0.381	-0.019	-0.025	0.130	0.092	0.281	0.208	-0.005		-0.012		-0.003	
3	0.092	0.087	0.240	0.202	0.388	0.317	-0.018	-0.024	0.108	0.070	0.237	0.164	-0.004		-0.012		0.001	
2	0.075	0.071	0.193	0.158	0.313	0.248	-0.017	-0.022	0.083	0.048	0.187	0.120	-0.004		-0.011		0.008	
1	0.053	0.050	0.128	0.102	0.161	0.114	-0.012	-0.016	0.051	0.025	0.120	0.072	-0.002		-0.008		0.009	
0	0.007	0.005	0.008	-0.011	0.012	-0.024	-0.001	-0.004	-0.001	-0.020	0.000	-0.036	-0.001		-0.006		-0.002	
4	0.087	0.086	0.238	0.232	0.381	0.369	-0.017	-0.018	0.115	0.109	0.244	0.232	-0.003		-0.002		-0.010	
8	0.134	0.132	0.379	0.360	0.606	0.570	-0.018	-0.021	0.197	0.178	0.404	0.368	-0.005		-0.006		-0.016	
4	0.103	0.101	0.276	0.257	0.442	0.406	-0.019	-0.022	0.131	0.112	0.279	0.243	-0.004		-0.006		-0.004	
0	0.004	0.004	0.003	0.006	0.004	0.010	0.000	0.000	0.000	0.003	0.000	0.000	0.000		0.001		0.000	

TABLE 4

Deflections of Strut 2F versus Load with One Loading Block

LOAD ($lb \times 10^{-3}$)	Indicator Number – Actual Displacement in Inches									
	1	2	3	4	5	6	7	8	9	10
0	0.000	0.000	0.000	0.000	0.000	0.000	0.000	0.000	0.000	0.000
5	0.023	0.058	0.108	0.021	0.053	0.099	-0.009	-0.013	0.022	–
10	0.041	0.103	0.192	0.034	0.089	0.179	-0.013	-0.019	0.026	–
15	0.065	0.155	0.284	0.049	0.130	0.260	-0.019	-0.032	–	0.000
20	0.079	0.195	0.361	0.062	0.162	0.334	-0.025	-0.042	0.035	0.000
25	0.094	0.232	0.435	0.078	0.204	0.404	-0.029	-0.050	0.038	0.000
30	0.110	0.273	0.509	0.093	0.242	0.479	-0.033	-0.061	0.040	0.000
30	0.125	0.297	0.550	0.099	0.258	0.513	-0.033	-0.070	0.043	-0.006
35	0.135	0.327	0.615	0.112	0.293	0.576	-0.037	-0.075	0.047	-0.007
40	0.150	0.369	0.696	0.129	0.335	0.655	-0.042	-0.086	0.052	-0.008
45	0.170	0.416	0.784	0.148	0.381	0.749	-0.049	-0.098	0.057	-0.011
50	0.187	0.464	0.876	0.165	0.428	0.839	-0.055	-0.109	0.059	-0.014
55	0.211	0.518	0.979	0.187	0.481	0.940	-0.064	-0.125	0.059	-0.024
60	0.231	0.570	1.084	0.206	0.532	1.046	-0.073	-0.144	0.059	-0.023

TABLE 5

Deflections of Strut 2F versus Load for Endsection Test

LOAD ($lb \times 10^{-3}$)	Indicator Number – Actual Displacement in Inches									
	1	2	3	4	5	6	7	8	9	10
0	0.000	0.000	0.000	0.000	0.000	0.000	0.000	0.000	0.000	0.000
1	0.044	0.085	0.142	0.050	0.091	0.138	-0.010	-0.020	0.010	0.000
2	0.064	0.122	0.206	0.065	0.130	0.202	-0.015	-0.023	0.018	0.000
3	0.081	0.160	0.268	0.080	0.170	0.258	-0.019	-0.027	0.024	0.000
4	0.100	0.201	0.332	0.096	0.203	0.313	-0.023	-0.033	0.027	0.000
5	0.116	0.235	0.388	0.110	0.235	0.362	-0.022	-0.031	0.030	0.000
6	0.132	0.269	0.440	0.123	0.271	0.414	-0.029	-0.035	0.031	0.000
3	0.082	0.152	0.249	0.082	0.085	0.245	-0.020	-0.025	0.025	0.000
6	0.133	0.261	0.431	0.124	0.183	0.407	-0.029	-0.034	0.034	0.000
7	0.148	0.291	0.474	0.136	0.294	0.447	-0.031	-0.037	0.035	0.000
8	0.164	0.323	0.523	0.151	0.326	0.495	-0.033	-0.038	0.036	0.000
9	0.179	0.351	0.562	0.164	0.357	0.534	-0.037	-0.048	0.036	0.000
10	0.194	0.380	0.599	0.176	0.388	0.575	-0.039	-0.055	0.036	0.000
11	0.209	0.411	0.650	0.189	0.421	0.626	-0.041	-0.060	0.036	0.000
12	0.226	0.445	0.697	0.202	0.454	0.675	-0.044	-0.064	0.035	0.000

REFERENCES

1. Bisplinghoff, R.L. et al., "Aeroelasticity," Addison-Wesley, Cambridge (1955).

2. Macovsky, M.S. et al., "An Investigation of a Flow-Excited Vibration of the USS FORREST SHERMAN (DD 931)," David Taylor Model Basin Report 1188 (Aug 1958).

3. Sverdrup, H.U. et al., "The Oceans," Prentice-Hall, Inc., Englewood Cliffs, N.J. (1942).

INITIAL DISTRIBUTION

Copies	
1	Air Force Office of Aerospace Research, Temporary Bldg D Washington 25, D.C.
9	NAVSHIPS 1 NAVSHIPS 0341C 3 NAVSHIPS 2051 2 NAVSHIPS 6114C 2 NAVSHIPS 6120 1 NAVSHIPS 6136
5	NURDC, San Diego, Code D551
1	CHONR, Fluid Dynamics Branch Code 438
1	Commander Research & Tech Div Air Force Flight Dynamics Lab W-PAFB Attn: Mr. Walter Mykytow
20	DDC
1	Commander NWC, China Lake
2	Commander, Pasadena Annex NUWC, Pasadena
1	Commander, NOL White Oak
1	Commanding Officer Office of Naval Research, Branch Office 495 Summer Street Boston 10, Mass
1	Commanding Officer Office of Naval Research, Branch Office 297 West 24th St New York 11, N.Y.
1	Commanding Officer Office of Naval Research, Branch Office 1030 East Green Street Pasadena 1, Calif
1	Commanding Officer Office of Naval Research, Branch Office 1000 Geary St San Francisco 9, Calif
1	Commanding Officer Office of Naval Research, Branch Office 219 South Dearborn St Chicago 1, Ill.
2	Director, Langley Research Center, Langley Field, Va. 1 Mr. I.E. Garrick 1 Mr. D.J. Martin
2	BUSTAND 1 Dr. G.B. Schubauer Chief, Fluid Mechanics Section 1 Dr. J.M. Frankland, Consultant
1	Office of Technical Services OTS, Dept of Commerce
1	Administrator U.S. Maritime Administration Attn: Mr. R.P. Godwin, Acting Chief Office of R&D
1	Accurate Products Co, Inc. 400 Hillside Ave Hillside, N.J.
2	The Boeing Co Aerospace Div P.O. Box 3707 Seattle 24, Wash Attn: Mr. R.R. Barber Lib Unit Chief
1	The Boeing Co Seattle Div Attn: Mr. F.B. Watson
1	Univ of Calif Dept of Engr Inst of Engr Research Berkeley 4, Calif Attn: Dr. J.V. Wehausen
3	CIT, Pasadena, Calif Attn: 1 Dr. M.S. Plesset 1 Dr. T.Y. Wu 1 Dr. A.J. Acosta

Copies	
1	Carnegie Inst of Technology Schenley Park Pittsburgh 13, Pa
1	Colorado State Univ Engr Research Div Fort Collins, Colorado
2	Convair P.O. Box 1950 San Diego 12, Calif 1 Mr. R. Peller 1 Mr. H.T. Brooks
1	Univ of Connecticut School of Engr Storrs, Connecticut
1	Cornell Aeronautical Lab, Inc. P.O. Box 235 Buffalo, N.Y. 14221
1	Douglas Aircraft Co El Segundo Div El Segundo, Calif
1	Edo Corp. College Point 56, N.Y.
1	Electric Boat Co General Dynamics Corp Groton, Conn Attn: Mr. Robert McCandliss
1	Editor, Engineering Index Engr Societies Lib 29 West 39th St New York 18, N.Y.
1	General Applied Sci Labs, Inc. Merrick & Stewart Avenues Westbury, L.I., N.Y. Attn: Dr. F. Lane
1	Gibbs & Cox, Inc.
1	Grumman Aircraft Engr Corp Dynamic Developments Div Babylon, N.Y.
2	Grumman Aircraft Engr Corp Bethpage, L.I., N.Y. Attn: Mr. E. Baird Mr. C. Squires
1	Hoerner (Gibbs & Cox) 148 Busteed Drive Midland Park, N.J.

Copies	
1	Hydro Space Div 3775 Sheridge Drive Sherman Oaks, Calif
2	President Hydronautics Inc. Pindell School Road Laurel, Md
1	Univ of Illinois College of Engr Urbana, Illinois
1	State Univ of Iowa Iowa Inst of Hydraulic Res Iowa City, Iowa Attn: Prof L. Landweber
1	Kaman Aircraft Corp Old Windsor Rd Bloomfield, Conn Attn: Mr. A. Lemnios
1	Library of Congress
1	Lockheed Missiles & Space Co Sunnyvale, Calif Attn: Mr. R.L. Waid
1	Univ of Md Dept of Mechanical Engr College Park, Md Attn: Dr. P.F. Cunniff
1	MIT, Div of Sponsored Res Cambridge 39, Mass
3	MIT, Fluid Dynamics Res Lab Cambridge 39, Mass 1 Prof H. Ashley 1 Prof M. Landahl 1 Dr. S. Widnall
1	Univ of Michigan Dept of Naval Arch & Marine Engr Ann Arbor, Michigan Attn: Prof. R.B. Couch
1	Midwest Research Institute 425 Volker Blvd Kansas City 10, Missouri Attn: Mr. Zeydel
2	Univ of Minn St. Anthony Falls Hydraulic Lab, Minneapolis 14, Minn Attn: Prof B. Silberman Mr. J.N. Wetzel

Copies

1 NYU, College of Engr
Univ Heights
New York 53, N.Y.

1 Northern Research & Engr Corp
Cambridge, Mass
Attn: Mr. James E. Smith

1 Univ of Notre Dame
Dept of Engr Mechanics
Notre Dame, Indiana

1 Oceanics, Inc.
Technical Industrial Park
Plainview, L.I., N.Y.
Attn: Dr. P. Kaplan

1 Ordnance Research Lab
Penn State Univ
Univ Park, Pa
Attn: Dr. M. Sevik

1 Princeton Univ
Dept of Aeronautical Engr
Princeton, N.J.
Attn: Prof. E.J. Brunelle

1 The Rand Corp
1700 Main St
Santa Monica, Calif
Attn: Dr. B. Parkin

1 Librarian, SNAME
74 Trinity Place
New York 6, N.Y.

3 SWRI, 8500 Culebra Rd
San Antonio 6, Texas
Attn: 1 Dr. H.N. Abramson
1 Mr. G. Ransleben
1 Editor, Applied
Mechanics Review

1 Sperry Gyroscope Co
Marine Div
7 Aerial Way
Syosset, L.I., N.Y.

2 Stanford Univ
Dept of Civil Engr
Stanford, Calif
Attn: 1 Dr. B. Perry
1 Dr. E.Y. Hsu

Copies

2 SIT, Davidson Lab
Castle Point Station
Hoboken, N.J.
Attn: 1 Mr. C.J. Henry
1 Mr. S. Taskonas

1 Robert Taggart, Inc.
Marine Sciences Bldg
3930 Walnut St
Fairfax, Va

7 TRG, Route 110, Melville
Long Island, N.Y.
Attn: 1 Dr. J. Kotik
1 Prof. S. Karp
3 Mr. I. Melnick
1 Mr. N. Weingart
1 Mr. G. Samis

1 Texas A&M Research Foundation
College Station, Texas

1 Therm Advanced Research
Div of Therm
Ithaca, N.Y.

1 WHOI, Woods Hole, Mass

UNCLASSIFIED

Security Classification

DOCUMENT CONTROL DATA - R & D

Security classification of title, body of abstract and indexing annotation must be entered when the overall report is classified)

1 ORIGINATING ACTIVITY (Corporate author)	2a. REPORT SECURITY CLASSIFICATION
Naval Ship Research & Development Center Washington, D.C. 20007	UNCLASSIFIED
	2b. GROUP

3 REPORT TITLE

HYDRODYNAMIC LOADING AND CAVITATION ON FIXED AND ROTATING STRUTS OF 25 PERCENT THICKNESS

4 DESCRIPTIVE NOTES (Type of report and inclusive dates)

Final

5 AUTHOR(S) (First name, middle initial, last name)

David W. Coder

6 REPORT DATE	7a. TOTAL NO OF PAGES	7b. NO OF REFS
December 1969	68	3

8a CONTRACT OR GRANT NO	9a. ORIGINATOR'S REPORT NUMBER(S)
b. PROJECT NO SS 048, Task 08543	2780
c. S 4606X, Task 1703	9b. OTHER REPORT NO(S) (Any other numbers that may be assigned this report)
d.	

10 DISTRIBUTION STATEMENT

This document has been approved for public release and sale; its distribution is unlimited.

11 SUPPLEMENTARY NOTES	12 SPONSORING MILITARY ACTIVITY
	Naval Ship Systems Command Washington, D.C.

13 ABSTRACT

Experimental results are presented for various towed struts of TMB-EPH cross section and thickness ratio of 25 percent. Force coefficients, strut accelerations, and cavitation characteristics as functions of velocity and angle of attack are given for a fixed strut of strong construction and a pinned rotating strut of weaker construction. The dynamics are given for rotating struts with axes of rotation at 18 percent chord with and without a splitter plate on the trailing edge. Test results obtained in fresh water at a depth of 1 ft are used to predict the behavior of the struts in sea water at a depth of 15 ft.

DD FORM 1 NOV 65 1473 (PAGE 1)

S/N 0101-807-6801

UNCLASSIFIED

Security Classification

14 KEY WORDS	LINK A		LINK B		LINK C	
	ROLE	WT	ROLE	WT	ROLE	WT
Struts, Rotating						
Struts, Nonrotating						
Hydrodynamic Loading						
Cavitation						
Struts, of 25 Percent Thickness						

Naval Ship R&D Center. Report 2780.
HYDRODYNAMIC LOADING AND CAVITATION ON FIXED AND ROTATING STRUTS OF 25 PERCENT THICKNESS, by David W. Coder. Dec 1969. vi, 62p. illus., refs.
UNCLASSIFIED

Experimental results are presented for various towed struts of TMB-EPH cross section and thickness ratio of 25 percent. Force coefficients, strut accelerations, and cavitation characteristics as functions of velocity and angle of attack are given for a fixed strut of strong construction and a pinned rotating strut of weaker construction. The dynamics are given for rotating struts with axes of rotation at 18 percent chord with and without a splitter plate on the trailing edge. Test results

1. Towed struts--Hydrodynamic loading
2. Towed struts--Cavitation
3. Towed struts (Rotating)--Hydrodynamic loading
4. Towed struts (Rotating)--Cavitation
I. Coder, David W.

Naval Ship R&D Center. Report 2780.
HYDRODYNAMIC LOADING AND CAVITATION ON FIXED AND ROTATING STRUTS OF 25 PERCENT THICKNESS, by David W. Coder. Dec 1969. vi, 62p. illus., refs.
UNCLASSIFIED

Experimental results are presented for various towed struts of TMB-EPH cross section and thickness ratio of 25 percent. Force coefficients, strut accelerations, and cavitation characteristics as functions of velocity and angle of attack are given for a fixed strut of strong construction and a pinned rotating strut of weaker construction. The dynamics are given for rotating struts with axes of rotation at 18 percent chord with and without a splitter plate on the trailing edge. Test results

1. Towed struts--Hydrodynamic loading
2. Towed struts--Cavitation
3. Towed struts (Rotating)--Hydrodynamic loading
4. Towed struts (Rotating)--Cavitation
I. Coder, David W.

Naval Ship R&D Center. Report 2780.
HYDRODYNAMIC LOADING AND CAVITATION ON FIXED AND ROTATING STRUTS OF 25 PERCENT THICKNESS, by David W. Coder. Dec 1969. vi, 62p. illus., refs.
UNCLASSIFIED

Experimental results are presented for various towed struts of TMB-EPH cross section and thickness ratio of 25 percent. Force coefficients, strut accelerations, and cavitation characteristics as functions of velocity and angle of attack are given for a fixed strut of strong construction and a pinned rotating strut of weaker construction. The dynamics are given for rotating struts with axes of rotation at 18 percent chord with and without a splitter plate on the trailing edge. Test results

1. Towed struts--Hydrodynamic loading
2. Towed struts--Cavitation
3. Towed struts (Rotating)--Hydrodynamic loading
4. Towed struts (Rotating)--Cavitation
I. Coder, David W.

Naval Ship R&D Center. Report 2780.
HYDRODYNAMIC LOADING AND CAVITATION ON FIXED AND ROTATING STRUTS OF 25 PERCENT THICKNESS, by David W. Coder. Dec 1969. vi, 62p. illus., refs.
UNCLASSIFIED

Experimental results are presented for various towed struts of TMB-EPH cross section and thickness ratio of 25 percent. Force coefficients, strut accelerations, and cavitation characteristics as functions of velocity and angle of attack are given for a fixed strut of strong construction and a pinned rotating strut of weaker construction. The dynamics are given for rotating struts with axes of rotation at 18 percent chord with and without a splitter plate on the trailing edge. Test results

1. Towed struts--Hydrodynamic loading
2. Towed struts--Cavitation
3. Towed struts (Rotating)--Hydrodynamic loading
4. Towed struts (Rotating)--Cavitation
I. Coder, David W.

obtained in fresh water at a depth of 1 ft are used to predict the behavior of the struts in sea water at a depth of 15 ft.

obtained in fresh water at a depth of 1 ft are used to predict the behavior of the struts in sea water at a depth of 15 ft.

obtained in fresh water at a depth of 1 ft are used to predict the behavior of the struts in sea water at a depth of 15 ft.

obtained in fresh water at a depth of 1 ft are used to predict the behavior of the struts in sea water at a depth of 15 ft.

Naval Ship R&D Center. Report 2780.
HYDRODYNAMIC LOADING AND CAVITATION ON FIXED AND ROTATING STRUTS OF 25 PERCENT THICKNESS, by David W. Coder. Dec 1969. vi, 62p. illus., refs.
UNCLASSIFIED

Experimental results are presented for various towed struts of TMB-EPH cross section and thickness ratio of 25 percent. Force coefficients, strut accelerations, and cavitation characteristics as functions of velocity and angle of attack are given for a fixed strut of strong construction and a pinned rotating strut of weaker construction. The dynamics are given for rotating struts with axes of rotation at 18 percent chord with and without a splitter plate on the trailing edge. Test results

1. Towed struts--Hydrodynamic loading
2. Towed struts--Cavitation
3. Towed struts (Rotating)--Hydrodynamic loading
4. Towed struts (Rotating)--Cavitation
I. Coder, David W.

Naval Ship R&D Center. Report 2780.
HYDRODYNAMIC LOADING AND CAVITATION ON FIXED AND ROTATING STRUTS OF 25 PERCENT THICKNESS, by David W. Coder. Dec 1969. vi, 62p. illus., refs.
UNCLASSIFIED

Experimental results are presented for various towed struts of TMB-EPH cross section and thickness ratio of 25 percent. Force coefficients, strut accelerations, and cavitation characteristics as functions of velocity and angle of attack are given for a fixed strut of strong construction and a pinned rotating strut of weaker construction. The dynamics are given for rotating struts with axes of rotation at 18 percent chord with and without a splitter plate on the trailing edge. Test results

1. Towed struts--Hydrodynamic loading
2. Towed struts--Cavitation
3. Towed struts (Rotating)--Hydrodynamic loading
4. Towed struts (Rotating)--Cavitation
I. Coder, David W.

Naval Ship R&D Center. Report 2780.
HYDRODYNAMIC LOADING AND CAVITATION ON FIXED AND ROTATING STRUTS OF 25 PERCENT THICKNESS, by David W. Coder. Dec 1969. vi, 62p. illus., refs.
UNCLASSIFIED

Experimental results are presented for various towed struts of TMB-EPH cross section and thickness ratio of 25 percent. Force coefficients, strut accelerations, and cavitation characteristics as functions of velocity and angle of attack are given for a fixed strut of strong construction and a pinned rotating strut of weaker construction. The dynamics are given for rotating struts with axes of rotation at 18 percent chord with and without a splitter plate on the trailing edge. Test results

1. Towed struts--Hydrodynamic loading
2. Towed struts--Cavitation
3. Towed struts (Rotating)--Hydrodynamic loading
4. Towed struts (Rotating)--Cavitation
I. Coder, David W.

Naval Ship R&D Center. Report 2780.
HYDRODYNAMIC LOADING AND CAVITATION ON FIXED AND ROTATING STRUTS OF 25 PERCENT THICKNESS, by David W. Coder. Dec 1969. vi, 62p. illus., refs.
UNCLASSIFIED

Experimental results are presented for various towed struts of TMB-EPH cross section and thickness ratio of 25 percent. Force coefficients, strut accelerations, and cavitation characteristics as functions of velocity and angle of attack are given for a fixed strut of strong construction and a pinned rotating strut of weaker construction. The dynamics are given for rotating struts with axes of rotation at 18 percent chord with and without a splitter plate on the trailing edge. Test results

1. Towed struts--Hydrodynamic loading
2. Towed struts--Cavitation
3. Towed struts (Rotating)--Hydrodynamic loading
4. Towed struts (Rotating)--Cavitation
I. Coder, David W.

obtained in fresh water at a depth of 1 ft are used to predict the behavior of the struts in sea water at a depth of 15 ft.

obtained in fresh water at a depth of 1 ft are used to predict the behavior of the struts in sea water at a depth of 15 ft.

obtained in fresh water at a depth of 1 ft are used to predict the behavior of the struts in sea water at a depth of 15 ft.

obtained in fresh water at a depth of 1 ft are used to predict the behavior of the struts in sea water at a depth of 15 ft.